Journal of Visualized Experiments

Exploring mitochondrial energy metabolism of single 3D microtissue spheroids using extracellular flux analysis
--Manuscript Draft--

Article Type:	Invited Methods Collection - JoVE Produced Video
Manuscript Number:	JoVE63346R2
Full Title:	Exploring mitochondrial energy metabolism of single 3D microtissue spheroids using extracellular flux analysis
Corresponding Author:	Jonathan Barlow UNITED KINGDOM
Corresponding Author's Institution:	
Corresponding Author E-Mail:	j.p.barlow@bham.ac.uk
Order of Authors:	Nicolas Coltman
	Garret Rochford
	Nikolas Hodges
	Hanene Ali-Boucetta
	Jonathan Barlow
Additional Information:	
Question	**Response**
Please specify the section of the submitted manuscript.	Cancer Research
Please indicate whether this article will be Standard Access or Open Access.	Standard Access ($1400)
Please indicate the **city, state/province, and country** where this article will be **filmed**. Please do not use abbreviations.	Birmingham, UK
Please confirm that you have read and agree to the terms and conditions of the author license agreement that applies below:	I agree to the Author License Agreement
Please confirm that you have read and agree to the terms and conditions of the video release that applies below:	I agree to the Video Release
Please provide any comments to the journal here.	

1 **TITLE:**
2 Exploring Mitochondrial Energy Metabolism of Single 3D Microtissue Spheroids Using
3 Extracellular Flux Analysis
4
5 **AUTHORS AND AFFILIATIONS:**
6 Coltman, N. J.[1], Rochford, G.[1], Hodges, N. J.[1], Ali-Boucetta, H.[2], Barlow, J. P.[3]
7
8 Coltman, N. J.   ORCID iD: https://orcid.org/0000-0002-8210-9178
9 Rochford, G.   ORCID iD: https://orcid.org/0000-0002-3291-403Xa
10 Hodges, N. J.   ORCID iD: https://orcid.org/0000-0002-3306-7688
11 Ali-Boucetta, H.   ORCID iD: https://orcid.org/0000-0002-5175-5716
12 Barlow, J. P.   ORCID iD: https://orcid.org/0000-0002-9463-7234
13
14 [1]School of Biosciences, University of Birmingham, Edgbaston, UK
15 [2]Nanomedicine, Drug Delivery & Nanotoxicology Lab, School of Pharmacy, University of
16 Birmingham, Edgbaston, UK
17 [3]Mitochondrial Profiling Centre, University of Birmingham, Edgbaston, UK
18
19 **Email addresses of co-authors:**
20 Coltman, N. J.   (NJC580@student.bham.ac.uk)
21 Rochford, G.   (garret2400@gmail.com)
22 Hodges, N. J.   (N.HODGES@bham.ac.uk)
23 Ali-Boucetta, H.   (H.AliBoucetta@bham.ac.uk)
24
25 **Corresponding author:**
26 Barlow, J. P.   (j.p.barlow@bham.ac.uk)
27

28 **SUMMARY:**
29 These protocols will help users probe mitochondrial energy metabolism in 3D cancer cell-line-
30 derived spheroids using Seahorse extracellular flux analysis.
31
32 **ABSTRACT:**
33 Three-dimensional (3D) cellular aggregates, termed spheroids, have become the forefront of *in*
34 *vitro* cell culture in recent years. In contrast to culturing cells as two-dimensional, single-cell
35 monolayers (2D culture), spheroid cell culture promotes, regulates, and supports physiological
36 cellular architecture and characteristics that exist *in vivo*, including the expression of extracellular
37 matrix proteins, cell signaling, gene expression, protein production, differentiation, and
38 proliferation. The importance of 3D culture has been recognized in many research fields,
39 including oncology, diabetes, stem cell biology, and tissue engineering. Over the last decade,
40 improved methods have been developed to produce spheroids and assess their metabolic
41 function and fate.
42
43 Extracellular flux (XF) analyzers have been used to explore mitochondrial function in 3D
44 microtissues such as spheroids using either an XF24 islet capture plate or an XFe96 spheroid

45   microplate. However, distinct protocols and the optimization of probing mitochondrial energy
46   metabolism in spheroids using XF technology have not been described in detail. This paper
47   provides detailed protocols for probing mitochondrial energy metabolism in single 3D spheroids
48   using spheroid microplates with the XFe96 XF analyzer. Using different cancer cell lines, XF
49   technology is demonstrated to be capable of distinguishing between cellular respiration in 3D
50   spheroids of not only different sizes but also different volumes, cell numbers, and DNA content
51   and type.
52
53   The optimal mitochondrial effector compound concentrations of oligomycin, BAM15, rotenone,
54   and antimycin A are identified to probe specific parameters of mitochondrial energy metabolism
55   in 3D spheroids. This paper also discusses methods to normalize data obtained from spheroids
56   and addresses many considerations that should be considered when exploring spheroid
57   metabolism using XF technology. This protocol will open further research avenues to identify
58   novel anticancer therapeutic modalities in 3D tumor spheroids.
59

60   **INTRODUCTION:**
61   Advances in *in vitro* models in biological research have rapidly progressed over the last 20 years.
62   Such models now include organ-on-a-chip modalities, organoids, and 3D microtissue spheroids,
63   all of which have become a common focus to improve the translation between *in vitro* and *in vivo*
64   studies. The use of advanced *in vitro* models, particularly spheroids, spans several research fields,
65   including tissue engineering, stem cell research, cancer, and disease biology[1-7], and safety testing,
66   including genetic toxicology[8-10], nanomaterials toxicology[11-14], and drug safety and efficacy
67   testing[8,15-19].
68

69   Normal cell morphology is critical to biological phenotype and activity. Culturing cells into 3D
70   microtissue spheroids allows cells to adopt a morphology, phenotypic function, and architecture,
71   more akin to that observed *in vivo* but difficult to capture with classical monolayer cell culture
72   techniques. Both *in vivo* and *in vitro,* cellular function is directly impacted by the cellular
73   microenvironment, which is not limited to cellular communication and programming (e.g., cell-
74   cell junction formations, opportunities to form cell niches); cell exposure to hormones and
75   growth factors in the immediate environments (e.g., cellular cytokine exposure as part of an
76   inflammatory response); composition of physical and chemical matrices (e.g., whether cells are
77   grown in stiff tissue culture plastic or an elastic tissue environment); and most importantly, how
78   cellular metabolism is impacted by nutrition and access to oxygen as well as the processing of
79   metabolic waste products such as lactic acid.
80

81   Metabolic flux analysis is a powerful way to examine cellular metabolism within defined *in vitro*
82   systems. Specifically, XF technology allows for the analysis of live, real-time changes in cellular
83   bioenergetics of intact cells and tissues. Given that many intracellular metabolic events occur
84   within the order of seconds to minutes, real-time functional approaches are paramount for
85   understanding real-time changes in cellular metabolic flux in intact cells and tissues *in vitro*.
86

87   This paper provides protocols for cultivating cancer-derived cell lines A549 (lung
88   adenocarcinoma), HepG2/C3A (hepatocellular carcinoma), MCF-7 (breast adenocarcinoma), and

89 SK-OV-3 (ovarian adenocarcinoma) as *in vitro* 3D spheroid models using forced-aggregation
90 approaches (**Figure 1**). It also (i) describes in detail how to probe mitochondrial energy
91 metabolism of single 3D spheroids using the Agilent XFe96 XF analyzer, (ii) highlights ways to
92 optimize XF assays using single 3D spheroids, and (iii) discusses important considerations and
93 limitations of probing 3D spheroid metabolism using this approach. Most importantly, this paper
94 describes how datasets are collected that allow the calculation of oxygen consumption rate (OCR)
95 to determine oxidative phosphorylation and thus mitochondrial function in cellular spheroids.
96 Though not analyzed for this protocol, extracellular acidification rate (ECAR) is another parameter
97 that is measured alongside OCR data in XF experiments. However, ECAR is often poorly or
98 incorrectly interpreted from XF datasets. We provide a commentary as to the limitations of
99 calculating ECAR following basic approaches from the technology manufacturer.
100
101 **PROTOCOL:**
102
103 [INSERT FIGURE 1 HERE]
104
105 **1.   Cultivation of cancer cell lines as 3D *in vitro* spheroids**
106
107 [INSERT TABLE 1 HERE]
108
109 1.1.   Culture all cell lines using standard aseptic tissue culture technique and confirm that they
110 are free of mycoplasma using a suitable assay kit.
111
112 1.2.   Culture the cell lines in T75 tissue culture flasks or equivalent, using the recommended
113 medium (**Table 1**). Culture the cell lines to 65–80% confluency and passage them regularly up to
114 a maximum of 25 passages.
115
116 1.3.   Rinse the cell culture flasks twice in Dulbecco's modified phosphate-buffered saline
117 (DBPS).
118
119 1.4.   Detach the cells from the flasks with 3 mL of the cell dissociation reagent (see the **Table**
120 **of Materials**) for 5 min at 37 °C and confirm the detachment by microscopy.
121
122 1.5.   Aspirate the detached cell suspension gently to ensure a single-cell suspension and
123 deactivate the cell dissociation reagent with 7 mL of complete tissue culture medium.
124
125 1.6.   Collect the cells by centrifugation at 300 × *g* for 5 min, discard the supernatant, and
126 resuspend the cells in complete medium.
127
128 1.7.   Count the cells using a hemocytometer or an automated cell counter and titrate to the
129 desired cell density required for seeding.
130

131 NOTE: To seed an entire 96-well plate at 100 µL/well at 4×10^3 cells/well, cells should be titrated
132 to 4×10^4 cells/mL in a recommended volume of 12 mL.

133

134 1.8.   Decant the cell suspension into a sterile reservoir and dispense 100 µL of the cell
135 suspension into each well of a cell-repellent microplate using a multichannel pipettor.

136

137 NOTE: Only the inner 60 wells of a microplate should be seeded and the remainder filled with
138 DPBS. This will form an evaporation barrier, ensure spheroid homogeneity across the plate, and
139 minimize plate edge effects.

140

141 1.9.   Centrifuge spheroid microplates at $300 \times g$ for 15 min to force the cells into loose
142 aggregates.

143

144 1.10.   Incubate the plates at 37 °C, 5% CO_2 for a minimum of 3 days to ensure spheroid
145 formation.

146

147 1.11.   Perform phase-contrast microscopy using standardized laboratory practices to monitor
148 the growth of spheroids. Replenish the cell culture medium every 3 days or twice weekly by
149 performing a half-volume medium exchange.

150

151 **2.   Probing mitochondrial energy metabolism of single spheroids using Extracellular Flux**
152 **(XF) Technology**

153

154 2.1. Assay preparation (one day prior)

155

156 2.1.1.   Check spheroid viability using an inverted light microscope with phase contrast at 4x
157 magnification to ensure intact spheroid structure, morphology, and overall uniformity between
158 samples.

159

160 2.1.2.   Hydrate the sensor cartridge.

161

162 2.1.2.1.   Aliquot ~20 mL of the calibrant into a conical tube.

163

164 2.1.2.2.   Place the conical tube containing the calibrant in a non-CO_2 37 °C incubator
165 overnight.

166

167 2.1.2.3.   Remove the contents from the assay kit.

168

169 2.1.2.4.   Remove the sensor cartridge from the utility plate and place it upside down on
170 the worktop next to the utility plate.

171

172 2.1.2.5.   Pipette 200 µL of sterile ddH_2O into each well of the sensor cartridge utility plate
173 using a multichannel P300 pipette.

174

175   2.1.2.6.   Place the sensor cartridge on top of the utility plate.

177   2.1.2.7.   Check that the water level in each well is high enough to submerge the sensor
178   probes.

180   2.1.2.8.   Transfer the assembled sensor cartridge to a non-CO2 37 °C incubator and leave
181   it overnight.

183   NOTE: This step can be performed 12–72 h prior to assay commencement.

185   2.2. Coating of the spheroid assay microplate

187   2.2.1. Using aseptic techniques, add 30 µL/well of sterile Poly-D-Lysine (0.1 mg/mL) solution to
188   the spheroid microplate and incubate it for 30 min at room temperature.

190   2.2.2. Aspirate the solution from each well of the spheroid microplate, invert the plate, and tap
191   it firmly onto tissue paper to remove any residual solution.

193   2.2.3. Wash the plate twice with 200 µL/well of sterile ddH$_2$O.

195   2.2.4. After the final wash, invert the microplate and tap it firmly onto tissue paper to remove
196   any residual water.

198   2.2.5. Allow the plate to air-dry for 30 min before using or storing it at 4 °C for future use.

200   NOTE: The spheroid assay microplate should be coated with a molecular adhesive to ensure that
201   the spheroids are fixed at the bottom of the microplate. Without a molecular adhesive, spheroids
202   can become dislodged and interfere with assay results. Other molecular adhesives can also be
203   used as an alternative to Poly-D-Lysine for precoating plates. Precoated plates can be stored at 4
204   °C but should be left to equilibrate to room temperature before assay commencement.

206   2.3.   Preparation of XF Assay medium

208   2.3.1. Prepare XF RPMI medium, as detailed in **Table 1**, and sterile-filter with a 0.22 µm syringe
209   filter

211   2.4.   Assay preparation (1 h prior to assay)

213   2.4.1. Prewarm the supplemented XF RPMI assay medium to 37 °C.

215   2.4.2. Prewarm the coated spheroid assay microplate in a non-CO$_2$ 37 °C incubator or dry bath.

217   2.4.3. Prepare the sensor cartridge.

219 2.4.3.1.   Take out the conical tube containing the calibrant and the sensor cartridge from
220 the air incubator.
221
222 2.4.3.2.   Remove the sensor cartridge from the utility plate and place it upside down on
223 the work surface.
224
225 2.4.3.3.   Using a P300 multichannel pipette, aspirate the water from the utility plate and
226 discard it.
227
228 2.4.3.4.   Pour the calibrant solution into a sterile reagent reservoir and add 200 µL/well of
229 the prewarmed calibrant to the utility plate using a P300 multichannel pipette.
230
231 2.4.3.5.   Pick up the sensor cartridge and place it back on top of the utility plate, ensuring
232 the sensors are well submerged in the calibrant.
233
234 2.4.3.6.   Transfer the assembled sensor cartridge back into the non-CO_2 37 °C incubator
235 until ready to load the port injection solutions.
236
237 2.5.   Wash the spheroids with the assay medium.
238
239 2.5.1.   Remove the spheroid culture plate from the 37 °C, 5% CO_2 incubator and observe the
240 spheroids under the microscope to ensure their integrity prior to the spheroid transfer steps.
241
242 2.5.2.   Load all wells of the spheroid plate with 180 µL/well of prewarmed assay medium,
243 including any background correction wells.
244
245 2.5.3.   Partially fill a 7 cm Petri dish with 3 mL of the assay medium.
246
247 2.5.4.   Using a multichannel pipette loaded with wide orifice pipette tips, transfer the spheroids
248 from the 96-well culture plate into 7 cm Petri dishes by setting the pipettor at an aspiration
249 volume of 10–50 µL.
250
251 2.6.   Seeding single spheroids into the spheroid assay microplate
252
253 2.6.1.   Using a dissection microscope and a lightbox apparatus, transfer the spheroids from the
254 Petri dish to the spheroid assay microplate as detailed below.
255
256 2.6.1.1.   Set the volume of a single-channel pipettor fitted with a wide orifice pipette tip to
257 20 µL and carefully aspirate a single spheroid. Place the tip directly in the center of each well of
258 the spheroid assay microplate and allow gravity to elute a single spheroid into the center of each
259 well, i.e., do not expel any medium from the pipette tip and allow capillary action to withdraw
260 the spheroid from the pipette tip. To confirm elution, the contents of the pipettor can be pipetted
261 back into the 7 cm Petri dish under the microscope.
262

263 NOTE: Gravity elution of a single spheroid typically takes 15–30 s depending on spheroid
264 size/density. During this time, the pipettor should not be removed. Any background correction
265 wells should be free of spheroids and only contain assay medium. Under the microscope, confirm
266 the position of each spheroid—each spheroid should ideally be positioned within the center of
267 each well.

268
269 2.6.1.2.   Once all the spheroids have been transferred to the spheroid assay microplate,
270 transfer the plate to a non-CO_2 incubator at 37 °C for a minimum of 1 h prior to the assay.

271
272 **3. Preparation and loading of compounds into the sensor cartridge for XF assays**

273
274 [INSERT TABLE 2 HERE]

275
276 3.1.   Prepare the working stock concentrations of each compound as noted in **Table 2** using
277 fully supplemented, prewarmed XF RPMI assay medium.

278
279 3.2.   Orient the cartridge plate (coupled to the utility plate) column-wise, 1–12 from left to
280 right.

281
282 3.3.   If using a loading guide, place it atop the cartridge plate according to the well-loading
283 procedure, e.g., if port A is be loaded first, ensure that **A** is visible in the upper-left corner of the
284 guide.

285
286 3.4.   Transfer the working solution of each compound into a suitable reservoir and, using a
287 calibrated P100 multichannel pipette, dispense 20 μL into all corresponding ports. Repeat for
288 each compound into the remaining ports.

289
290 NOTE: If any ports are not used on the sensor cartridge plate, these can be left empty or filled
291 with assay medium. If only a selection of a specific port letter is being used, ensure that the other
292 ports corresponding to that letter are loaded with assay medium; otherwise, air will be injected
293 into the well, compromising the results in those wells.

294
295 3.5.   After port loading, remove the plate-loading guides (if used) and prepare the analyzer for
296 loading the sensor cartridge.

297
298 NOTE: If the assay is not being run immediately after loading the ports, place the lid back on the
299 sensor cartridge and put the plate back in the 37 °C air incubator until ready to load into the
300 machine.

301
302 **4.   Assay design, injection strategies, and data acquisition**

303
304 4.1.   Running the assay

305
306 4.1.1.   Power on the analyzer and connect to controller (computer).

307

308 NOTE: This can be verified by the instrument connection status in the widget panel of the Wave
309 Controller software.

310

311 4.1.2. Navigate to the **templates** page in the WAVE software, find the assay template file for the
312 experiment and double-click to open it.

313

314 NOTE: If the assay template does not appear on the **Templates** view, import the template file
315 into the template folder from a shared network drive or USB flash drive.

316

317 4.1.3. To start the assay, click the **Run Assay** tab.

318

319 NOTE: If the group definitions have been correctly allocated within the plate map, the assay will
320 be ready to run as indicated by the green tick on the right-hand side of the page. At this stage,
321 any additional information can be input on the assay summary page or the page left blank;
322 proceed to the next step. Due to the delayed penetration of mitochondrial modulators in 3D
323 microtissue spheroids (**Figure 2**), use the measurement protocol information described in **Table**
324 **3**.

325

326 [INSERT TABLE 3 HERE]

327

328 4.1.4. Click **start run** to bring up the **save location** dialog box.

329

330 4.1.5. Enter the **save location** for the result file, and place the assembled sensor cartridge onto
331 the thermal tray that appears from the door on the side of the analyzer. Wait for the thermal
332 tray to open automatically and the screen to display the **Load Calibrant Utility Plate** message.
333 Before following the on-screen prompts, ensure i) proper fit of the sensor cartridge on the Utility
334 plate, ii) the lid is removed from the sensor cartridge, and iii) correct orientation of the sensor
335 cartridge on the utility plate.

336

337 4.1.6. Follow the on-screen commands to initiate sensor cartridge calibration.

338

339 NOTE: The time taken to complete calibration is approximately 10–20 min (for assays at 37 °C).

340

341 4.1.7 After sensor cartridge calibration, load the spheroid microplate into the analyzer by
342 following the on-screen instructions on the Wave Controller to initiate the 12 min equilibration
343 step.

344

345 NOTE: Green boxes with white ticks indicate a 'good' calibration for that well. If any wells fail to
346 provide a 'good' calibration, they will be indicated with a red box and white cross. Such wells
347 should be noted and excluded from any analysis after the assay is completed using the
348 **modification assay** tab.

349

350 4.1.8   Wait for the analyzer to automatically begin acquiring baseline measurements after the
351 machine has completed the equilibration step (as outlined in the instrument protocol).
352
353 4.1.9   To complete the experiment, follow the on-screen commands on the WAVE controller.
354
355 NOTE: Once the spheroid microplate has been removed from the analyzer, discard the sensor
356 cartridge and set aside the spheroid plate for further analysis if necessary (e.g., double-stranded
357 (ds) DNA quantification). If the microplate is not required for further analysis, it can be discarded
358 along with the sensor cartridge.
359
360 4.1.10 Wait for the assay dialog to appear and view the results or return to the **templates** view.
361
362 **5. Data normalization and analysis strategies—post assay normalization and downstream**
363 **assays** (optional steps)
364
365 5.1. Data normalization
366
367 5.1.1. To normalize spheroid data, refer to the series of protocols pertinent to data normalization
368 strategies for calculating spheroid size and volume and quantifying ds DNA in spheroid assays.
369 These have been included as supplemental files; see **Supplemental file 1** and **Supplemental file**
370 **2**.
371
372 5.2. Data analysis
373
374 5.2.1. To export data into one of the automated analysis generators, follow the data export
375 commands on the WAVE controller and select the export generator that matches the assay type.
376 Alternatively, export the data file and upload it into Seahorse analytics.
377
378 NOTE: The downside of report generators and Seahorse analytics is that data analysis is limited
379 to how the XF assay is designed and does not allow for averages to be taken across measurement
380 cycles. Manual export of datasets from the instrument software allows for user preference in this
381 regard. Given that the injection strategy for assessing mitochondrial respiration of 3D spheroids
382 will likely differ from that of a typical 'MitoStress' test, a series of spreadsheet templates have
383 been developed to help analyze these datasets, specific to 3D cell cultures and will be provided
384 upon request. These data template files will provide data on the key mitochondrial respiratory
385 parameters detailed and explained in **Figure 2**.
386
387 5.2.2. To analyze the data, export the data as a spreadsheet report from the WAVE controller
388 software and use an independent spreadsheet template for analysis.
389

390 **[INSERT FIGURE 2 HERE]**

391
392 **REPRESENTATIVE RESULTS:**

393 To obtain well-formed, compact spheroids, each cell line was optimized individually for seeding
394 density and duration of cultivation (**Figure 3**). A549, HepG2/C3A, and SK-OV-3 cell lines initially
395 formed loose aggregates that did not progress to round spheroids with clearly defined perimeters
396 until after 7 days in culture. Conversely, MCF-7 cells could form spheroids within 3 days. There
397 was a clear correlation between the initial cell seeding density and spheroid volume after the
398 culture period for all spheroid models. Spheroid size and morphology were optimized to seeding
399 density. Morphology and circularity began to decline with increased spheroid size in all models.
400 Seeding strategies for cell lines were optimized at 4×10^3 cells/well for A549 and SK-OV-3 cells;
401 HepG2/C3A cells have been previously optimized elsewhere to 1×10^3 cells/well, and MCF-7 cells
402 were used at 4×10^3 cells/well in all assays. At optimized seeding strategies, spheroid volume
403 was between 5.46×10^7 μm^3 (SK-OV-3) and 1.45×10^8 μm^3 (A549) (**Figure 3B**). All spheroid types
404 had a linear correlation between the initial seeding density and spheroid volume where A549 and
405 HepG2/C3A had R^2 values of 0.957 and 0.947, respectively. MCF-7 and SK-OV-3 spheroid volumes
406 were both found to have a greater correlation with the initial seeding density, R^2=0.977 (**Figure
407 3A**).
408
409 Spheroid circularity was calculated using image planimetry within FIJI analysis software using the
410 long and short spheroid diameters. Perfect spheroid symmetry had circularity = 1.0; deviation
411 from 1.0 indicated a loss of circularity (**Figure 3C**). Circularity was greater in MCF-7 spheroids than
412 other models where circularity was maintained between 0.83 and 0.9 at all seeding densities. By
413 comparison, the outer perimeter of SK-OV-3 spheroids was not as clearly defined, and spheroid
414 volume was significantly smaller even after 7 days in culture, yielding spheroids with a maximum
415 circularity of 0.61 at a seeding density of 4×10^3/well. HepG2/C3A cells were also found to form
416 tight, well-formed spheroids with an even morphology across the surface area of all spheroids,
417 with circularity maintained at 0.79 for cells seeded at 1×10^3 cells/well. A549 cells appeared to
418 follow a trend wherein spheroid circularity and morphology were enhanced with seeding density;
419 however, circularity was not greater than 0.63 at the density used in these experiments.
420
421 Basal mitochondrial respiration was calculated as OCR measured from spheroids seeded at $1 \times$
422 10^3, 2×10^3, 4×10^3, or 8×10^3 cells/well in ultralow attachment spheroid culture microplates
423 (**Figure 3D**). For all spheroid types, OCR increased with spheroid size and was linearly correlated
424 to spheroid volume with R^2 highest in MCF-7 spheroids at 0.988 and lowest in SK-OV-3 spheroids
425 at 0.744 (**Figure 3E**). The measured OCR was statistically different between all experimental
426 groups. A549 had the lowest OCR, achieving only 18 pmol/min/well at the largest spheroid size
427 (**Figure 3D**). Conversely, MCF-7 spheroids yielded a similar OCR at the smallest spheroid size after
428 only 3 days in culture, reaching a maximum baseline OCR of 53 pmol/min/well for the largest
429 spheroid size (**Figure 3D**). HepG2/C3A yielded OCR data highly consistent with spheroid size and
430 morphology. In HepG2/C3A spheroids seeded from 1×10^3 cells/well, baseline OCR reached an
431 average of 15 pmol/min/well, increasing to a maximum of 52 pmol/min/well in the largest
432 spheroids (**Figure 3D**). OCR in SK-OV-3 spheroids was only significant between spheroids grown
433 from 4×10^3 cells/well and 8×10^3 cells/well, with little difference seen in spheroids grown
434 between 1×10^3, 2×10^3, or 4×10^3 cells. Despite size differences, OCR data were highly similar
435 between HepG2/C3A and MCF-7 cells at all size points. Relative to spheroid size (μm^3), baseline

436 OCR by MCF-7 spheroids was comparable to that of HepG2/C3A spheroids grown over 7 days
437 from 1,000 cells per well.

438

439 [PLACE FIGURE 3 HERE]

440

441 The concentration and time course for exposure to respiratory modulators in XF analysis is a
442 critical step in assay optimization. Respiratory modulator compounds—oligomycin, BAM15, a
443 mixture of rotenone–antimycin A—or a DMSO vehicle control were sequentially injected through
444 the sensor cartridge injection ports into microplate wells containing the MCF-7 spheroids (**Figure**
445 **4A**). Four measurement cycles were completed to determine the average basal OCR of 30–40
446 pmol/min/well for all sample groups. For the remainder of the assay duration, respiratory
447 modulators were sequentially added every 5 measurement cycles to achieve final well
448 concentrations of 0.5 µM (0.5 µg/mL oligomycin) after injection 1; 2.0 µM (2 µg/mL oligomycin)
449 after injection 2; 5 µM (5 µg/mL oligomycin) after injection 3; and finally, a maximum well
450 concentration of 11 µM (11 µg/mL oligomycin) after the fourth sequential addition. MCF-7
451 spheroids did not respond to the vehicle control throughout the experiment (**Figure 4A**). Basal
452 OCR immediately changed after the first injection of each respective compound at the lowest
453 concentration of 0.5 µM or 0.5 µg/mL oligomycin (**Figure 4B**). OCR in MCF-7 spheroids was
454 lowered with oligomycin from 41 pmol/min/well to 23 pmol/min/well after 5 measurement
455 cycles following the first injection of 0.5 µg/mL (**Figure 4B**).

456

457 In response to 0.5 µm BAM15, OCR was increased from 33 to 41 pmol/min/well before the
458 second injection (**Figure 4C**). Comparatively, the combination of rotenone plus antimycin A
459 lowered OCR from 37 to 13 pmol/min/well before the second injection (**Figure 4D**). Kinetic traces
460 further revealed a steady linear decrease (oligomycin and rotenone–antimycin A) or increase
461 (BAM15) in OCR. For all compound dosing regimens, a steady-state OCR was achieved within 10–
462 12 complete measurement cycles (60–72 min) at a total well concentration of 2 µM BAM15, 2
463 µM rotenone, 2 µM antimycin A, and 2 µg/mL oligomycin (**Figure 4A**). Oxygen consumption rate
464 reached a steady-state plateau at ~19 pmol/min/well (oligomycin), 52 pmol/min/well (BAM15),
465 and 10 pmol/min/well (rotenone–antimycin A) (**Figure 4A**). Increasing the compound
466 concentration of oligomycin, BAM15, or rotenone plus antimycin A further had no obvious effect
467 on OCR, which remained constant throughout the remainder of the assay. These data
468 demonstrate that both compound concentration and time course of exposure to respiratory
469 modulator compounds should be considered for assay optimization when using 3D spheroids.

470

471 [PLACE FIGURE 4 HERE]

472

473 One of the main benefits of XF technology is the ability to probe mitochondrial function in intact
474 cells and tissues. To examine specific aspects of mitochondrial function in cells and tissues,
475 mitochondrial modulators are added sequentially to wells of the sample microplate through the
476 4 available injection ports on the sensor cartridge. The typical sequence of modulators used to
477 probe mitochondrial parameters in XF assays are oligomycin, a protonophore (e.g., FCCP or
478 BAM15), and a combination of rotenone plus Antimycin A, which are added sequentially to inhibit

479 the mitochondrial ATP synthase, determine maximal respiratory capacity, and correct for
480 nonmitochondrial respiratory rate, respectively. This typical sequence of modulator additions is
481 termed the **MitoStress test** by the assay technology manufacturer. Given that oligomycin can
482 inhibit uncoupler-stimulated respiration in some cell monolayers[20], we examined this with
483 cancer-derived 3D spheroids by measuring uncoupled-stimulated OCR (OCR_{max}) before (single)
484 and after (sequential) oligomycin injection (**Figure 5A–D**). OCR_{max} was not significantly limited by
485 the addition of oligomycin in spheroids formed from HEPG2/C3A or SK-OV-3 (**Figure 5E** and
486 **Figure 5G**). However, OCR_{max} was significantly lowered in A549 and MCF-7 spheroids following a
487 sequential injection of BAM15 after oligomycin compared to OCR_{max} achieved from a single
488 injection of BAM15 (**Figure 5F** and **Figure 5H**). Unless otherwise known, it is therefore
489 recommended to use separate wells to treat with oligomycin and uncoupler, with a final addition
490 of rotenone and antimycin A when exploring mitochondrial energy metabolism of 3D spheroids.
491 This approach still allows for the calculation of all mitochondrial parameters as with a typical
492 **MitoStress test** where compounds are added sequentially.
493
494 **[PLACE FIGURE 5 HERE]**
495
496 Using optimal cell seeding densities, compound concentrations, injection strategy, and
497 measurement cycle period determined in these optimization experiments (**Table 3**), we have
498 developed a detailed protocol for accurately probing basal mitochondrial respiration: OCR_{basal}
499 (**Figure 6A**), ADP phosphorylation respiration: OCR_{ADP} (**Figure 6B**), leak respiration: OCR_{omy}
500 (**Figure 6C**), coupling efficiency (**Figure 6D**), maximal respiratory capacity: OCR_{max} (**Figure 6E**), and
501 spare respiratory capacity: OCR_{spare} (**Figure 6F**) using cancer-derived 3D spheroids.
502
503 **[PLACE FIGURE 6 HERE]**
504
505 MCF-7 spheroids grown from 4×10^3 cells/well over 3 days were used as a model to determine
506 optimum transfer, placement, and analysis within spheroid assay microplates. Using dimensions
507 provided for the spheroid microplate from the manufacturer, the well surface was split into three
508 zone-areas for optimum spheroid placement (**Figure 7A**), where zone 1 was highlighted as the
509 optimal zone at the center of the well. With careful pipetting using wide-orifice pipette tips,
510 spheroids were transferred into the spheroid plates and randomly distributed across the well-
511 surfaces by gravity elution (**Figure 7B**). Where spheroids were carefully transferred using gravity
512 elution, most spheroids could typically be found in zones 1–2 of the microplate, using the
513 recommended transfer techniques from the manufacturer. Where spheroids were forced out of
514 the pipette tip by aspiration, spheroids were often placed beyond these zones and could not be
515 seen using microscopy.
516
517 To compare spheroid placement positions, MCF-7 spheroids were transferred into the spheroid
518 assay microplates in designated zones 1–3 or out of zone (**Figure 7A**). These 4 wells were tracked
519 through a kinetic experiment OCR at baseline and after the addition of oligomycin, BAM15, or
520 rotenone–antimycin A (**Figure 7C**). OCR was calculated from the mean of three cycle readings
521 before each injection (**Figure 7B**). OCR was measured kinetically over 200 min in the 4 selected

522 wells (**Figure 7C**) and baseline-corrected (**Figure 7D**). Where spheroids were placed in zone 3 or
523 out of zone, baseline OCRs were significantly lower than spheroids placed in zones 1 and 2 (**Figure**
524 **7C**). The effects of respiratory compounds oligomycin, BAM15, and rotenone–antimycin A also
525 differed dramatically between spheroids placed in zones 1 and 2 compared with zone 3 and out-
526 of-zone regions. An increase in OCR was seen with oligomycin in spheroids placed in zone 3 or
527 out of zone (**Figure 7E**). Moreover, spheroids placed in zone 3 or out of zone experienced an
528 excessively high response to BAM15 with OCR higher than baseline following rotenone–
529 antimycin A injection (**Figure 7E**). Despite an almost two-fold increase in basal OCR (**Figure 7C**)
530 with spheroids placed in zone 2 versus zone 1, the fold-changes in response to all respiratory
531 compounds were very similar (**Figure 7E**), suggesting that differences in basal OCR between
532 spheroids placed in zones 1 or 2 are unlikely to be the result of placement within the well.
533
534 [PLACE FIGURE 7 HERE]
535
536 The selection criteria for the background are of high importance; the use of outermost wells for
537 background correction is not representative of all microplate wells, which may lead to incorrect
538 data assumptions being drawn and erroneous data conclusions due to edge effects across the
539 spheroid microplate. To assess this observation, MCF-7 spheroids were used to compare the
540 assay correction procedures to derive OCR values in response to the addition of a vehicle control,
541 oligomycin, BAM15, or rotenone–antimycin A (**Figure 8**). All respiratory compounds yielded the
542 expected kinetic OCR profiles for the selected compounds, revealing an average steady basal
543 respiration rate of 20–30 pmol/min/well (**Figure 8A**). However, where the assay data were
544 analyzed using the outermost wells for background temperature correction (A1, A12, H1, and
545 H12), values revealed for OCR after the addition of respiratory compounds were especially low;
546 OCR yielded negative values for rotenone–antimycin A. In response to these observations,
547 alternative analysis was performed using a series of empty wells, randomly distributed across the
548 spheroid microplate, as background temperature correction wells (**Figure 8B**). Where alternative
549 background correction was applied, all relative compound effects on OCR were the same in both
550 analysis sets; however, absolute OCR values increased by approximately 10 pmol/min/well
551 (**Figure 8**). These data highlight the power and importance of background temperature correction
552 on spheroid assay microplates and emphasize the importance of user optimization for XF
553 analysis.
554
555 [PLACE FIGURE 8 HERE]
556
557 Unlike cell monolayers, spheroids represent a heterogeneous aggregation of cells in a 3D space
558 and therefore require thorough consideration with respect to analysis, particularly when
559 normalizing these data. This paper presents three approaches to normalize XF data acquired from
560 MCF-7 spheroids (**Figure 9**). When unnormalized, OCR positively correlates (R^2 = 0.98) with
561 spheroid size (determined by initial cell seeding density) significantly when compared statistically
562 with Pearson correlation coefficient, P = 0.0057 (**Figure 9A**). This linear relationship is lowered
563 when OCR is normalized to the initial cell seeding density (R^2 = 0.78) and no longer significantly
564 correlates with spheroid size (P = 0.117, **Figure 9B**). This is also the case when normalized to

565 spheroid volume (R^2 = 0.77; Pearson correlation coefficient P = 0.120, **Figure 9C**) and nuclear
566 dsDNA content (R^2 = 0.58; Pearson correlation coefficient P= 0.233, **Figure 9D**). These data
567 highlight the importance of normalizing XF data when probing the mitochondrial metabolism of
568 spheroids, especially if they are of different sizes.
569
570 [PLACE FIGURE 9 HERE]
571
572 **FIGURE AND TABLE LEGENDS:**
573
574 **Figure 1: Graphical workflow for the generation of cellular spheroids, extracellular flux analysis,**
575 **downstream assays.** Four cancer cell lines were selectively cultured as monolayers (**A**), detached
576 from tissue culture flasks, and seeded into ultralow attachment 96-well microplates to form
577 spheroids (**B**). A549 lung carcinoma, HepG2/C3A liver carcinoma, SK-OV-3 ovarian
578 adenocarcinoma, and MCF-7 breast carcinoma cells were seeded at 1×10^3–8×10^3 cells/well and
579 grown up to 7 days to form single spheroids and optimize spheroid seeding density and
580 cultivation time by continuous observation and planimetric measurements. Once formed, single
581 spheroids were washed into a serum-free XF medium and carefully seeded into spheroid assay
582 microplates, precoated with poly-D-lysine (**C**). Spheroids were subjected to extracellular flux
583 analysis using the XFe96 analyzer using several protocols to address: (1) optimal spheroid size for
584 basal mitochondrial respiration response; (2) optimized titration of mitochondrial respiratory
585 inhibitors; (3) optimization of spheroid placement within microplate wells. (**D**) Post XF analyses,
586 phase contrast microscopy, and spheroid DNA quantification were used for data normalization
587 and other downstream *in vitro* assays.
588
589 **Figure 2: Schematic descriptors for parameters derived from extracellular flux data analyses.**
590 Abbreviation: OCR = oxygen consumption rate.
591
592 **Figure 3: Spheroid growth parameters determine baseline mitochondrial respiration.** (**A**) A549,
593 HepG2/C3A, MCF-7, and SK-OV-3 spheroids were optimized for seeding density and their growth
594 monitored at 1×10^3, 2×10^3, 4×10^3, and 8×10^3 cells/well in each of the photomicrographs,
595 from upper left to lower right, respectively; scale bars = 500 μm. (**B**) Spheroid size was calculated
596 using planimetric data from collected photomicrographs and compared using Pearson's
597 correlation statistic; dotted lines represent the distribution of 95% confidence interval. (**C**)
598 Spheroid morphology was compared by calculation of circularity. (**D**) OCR was measured 5x, after
599 which rotenone–antimycin A was added to account for nonmitochondrial respiratory rate using
600 the Agilent Seahorse XFe96 analyzer. OCR_{basal} measured as OCR – $OCR_{r/a}$ was compared between
601 seeding density (**D**) and spheroid volume (**E**). Data are averages ± SEM from 5–8 well replicates
602 per spheroid type and cell seeding density. Abbreviations: OCR = oxygen consumption rate;
603 OCR_{basal} = Basal mitochondrial respiration; $OCR_{r/a}$ = OCR after addition of rotenone–antimycin A.
604
605 **Figure 4: Titration of respiratory modulator compounds as an important step for optimizing**
606 **extracellular flux analysis.** (**A**) MCF-7 spheroids were seeded at 4×10^3 cells/well and cultured
607 over 3 days before being placed in wells of a spheroid assay microplate containing XF RPMI and

608   probed for OCR ± mitochondrial modulators using the XFe96 analyzer. OCR was measured 5x,
609   after which titrations of either vehicle control, oligomycin (**B**), BAM15 (**C**), or rotenone–antimycin
610   A (**D**) were added to inhibit mitochondrial ATP synthase, determine maximal respiratory capacity,
611   or establish nonmitochondrial respiratory rate, respectively. The concentration of each
612   mitochondrial modulator was increased over 4 individual titration injection strategies (0.5 µM,
613   1.5 µM, 3 µM, and 6 µM; units for oligomycin are µg/mL) to determine maximal steady-state OCR
614   in response to optimal compound concentration. OCR was measured for 5 measurement cycles
615   between each injection. Data are averages ± SEM from 5–8 individual well replicates.
616   Abbreviation: OCR = oxygen consumption rate.

617

618   **Figure 5: Single or sequential injection of mitochondrial respiratory compounds.** Cancer-cell-
619   derived spheroids of MCF-7, HEPG2/C3A, SK-OV-3, and A549 were placed into wells of an XFe96
620   spheroid microplate in XF RPMI and probed for OCR using the Agilent Seahorse XFe96 analyzer.
621   OCR was measured 5x, after which 2 µg/mL oligomycin (injection Port A: green trace) or 5 µM
622   BAM15 (injection Port A: blue trace or injection port B: green trace) to inhibit the mitochondrial
623   ATP synthase and determine maximal respiratory capacity, respectively. Kinetic OCR data are
624   expressed as % basal (**A–D**). Maximal respiratory capacity (OCR$_{max}$) was calculated as a factor of
625   basal OCR by the equation: OCR$_{max}$ = OCR$_{BAM15}$ / OCR$_{basal}$. OCR$_{max}$ was obtained from OCR averages
626   across measurement cycles 8–10 post BAM15 injection with (green bars) and without (blue bars)
627   oligomycin. Data are averages ± SEM from 3–8 individual well replicates across the spheroid assay
628   microplate. Abbreviations: OCR = oxygen consumption rate.

629

630   **Figure 6: Probing OCR with XF technology to establish mitochondrial energy metabolism of**
631   **cancer-derived spheroids.** Cancer-cell-derived spheroids of MCF-7, HEPG2/C3A, SK-OV-3, and
632   A549 were placed in wells of a spheroid assay microplate in XF RPMI and probed for OCR using
633   the Agilent Seahorse XFe96 analyzer. OCR was measured 5x, after which 2 µg/mL oligomycin, or
634   5 µM BAM15, and RA was added to inhibit the mitochondrial ATP synthase, determine maximal
635   respiratory capacity, and calculate the nonmitochondrial respiratory rate, respectively. (**A**) Basal
636   mitochondrial respiration (OCR$_{basal}$) was calculated as the average of OCR from the 3
637   measurement cycles before port A injection. (**B**) Coupling efficiency of oxidative phosphorylation
638   was approximated by expressing OCR$_{ADP}$ (OCR$_{basal}$ − OCR$_{leak}$) as a percentage of OCR$_{basal}$. (**C**) ADP
639   phosphorylation respiration (OCR$_{ADP}$) was measured as oligomycin-sensitive OCR, calculated
640   from the averaged OCR across measurement cycles 11–13 prior to BAM15 injection. (**D**) Leak$_{omy}$
641   respiration (OCR$_{leak}$) was measured as OCR insensitive to oligomycin, calculated from the mean
642   averaged OCR across measurement cycles 11–13. (**E**) Maximal respiratory capacity (OCR$_{max}$) was
643   measured as the average maximum OCR measured following BAM15 injection. (**F**) Spare
644   respiratory capacity was calculated by expressing OCR$_{spare}$ (OCR$_{max}$ − OCR$_{basal}$) as a percentage of
645   OCR$_{basal}$. OCR after rotenone–antimycin A injection (OCR$_{r/a}$) was subtracted from all rates to
646   correct for nonmitochondrial OCR. Data are averages ± SEM from 3–8 individual well replicates
647   across the XFe96 spheroid plate. Abbreviations: OCR = oxygen consumption rate; RA = 2 µM
648   rotenone–2 µM antimycin A.

649

650   **Figure 7: Placement of spheroids within the spheroid assay microplate dictates basal OCR and**
651   **mitochondrial modulator effects using XF technology.** MCF-7 spheroids were seeded at 4×10^3

652 cells/well and cultured over 3 days before being placed into the wells of the spheroid microplate
653 containing XF RPMI and probed for OCR ± mitochondrial modulators using the Agilent Seahorse
654 XFe96 analyzer. (**A**) Photomicrographs of spheroid zone positions in spheroid assay microplates
655 after assay duration; scale bar = 500 μm and OCR captured from corresponding wells over time
656 expressed as either pmol/min^{-1}/well^{-1} (**B**) or % basal (**C**). (**D**) Mitochondrial modulator effects of
657 MCF-7 spheroids placed in different zones within the spheroid assay microplate; data expressed
658 as fold change from basal. (**E**) Example kinetic trace highlighting which OCR data measurements
659 (red circles) are used to calculate the response of each mitochondrial modulator for data
660 presented in **E**. Data shown are from individual well responses. Abbreviation: OCR = oxygen
661 consumption rate.
662
663 **Figure 8: Random selection of wells for background correction to improve the control for**
664 **temperature gradients across the spheroid assay microplate.** OCR data extrapolated from
665 **Figure 2A** using recommended wells for background correction (**A**) versus randomly assigned
666 wells for background correction (**B**). Abbreviation: OCR = oxygen consumption rate.
667
668 **Figure 9: Normalization of extracellular flux data acquired from cellular spheroids.** (**A**) Raw OCR
669 data were obtained from MCF-7 cultured over 3 days and plotted using Pearson's model to obtain
670 a correlation coefficient between spheroid seeding density and OCR; *P* value set at 0.05. (**B**) Raw
671 OCR data were normalized against initial spheroid seeding density; (**C**) MCF-7 spheroid volume
672 obtained from microscopy planimetry; and (**D**) nuclear ds DNA content compared using Pearson's
673 correlation coefficient. Abbreviations: OCR = oxygen consumption rate; ds DNA = double-
674 stranded DNA.
675
676 **Table 1: Cancer cell line media and XF media compositions.**
677
678 **Table 2: Mitochondrial compound concentrations for probing mitochondrial energy**
679 **metabolism of single 3D spheroids using the XFe96 Analyzer.**
680
681 **Table 3: Protocol setup for probing mitochondrial energy metabolism of single 3D spheroids**
682 **using the XFe96 Analyzer.**
683
684 **Table 4: Optimized parameters for determining basal OCR measurements in single 3D**
685 **spheroids.** Abbreviation: OCR = oxygen consumption rate.
686
687 **Supplemental File 1: Analysis of spheroid size and volume.**
688
689 **Supplemental File 2: Quantification of double-stranded DNA from spheroids in the spheroid**
690 **microplate.**
691
692 **Supplemental File 3: Recommendations for the number of replicates required to obtain reliable**
693 **XF assay datasets.**
694
695 **DISCUSSION:**

Main findings and outputs

This paper provides a detailed protocol to probe mitochondrial energy metabolism of single 3D spheroids using a series of cancer-derived cell lines with the XFe96 XF Analyzer. A method is developed and described for the rapid cultivation of A549, HepG2/C3A, MCF7, and SK-OV-3 cellular spheroids using cell-repellent technologies for forced aggregation. This protocol addresses many considerations of probing spheroid metabolism with XF technology, including (1) optimization of spheroid culture protocols and the handling and transfer of spheroids into specific spheroid assay microplates from the technology manufacturer from their original culturing vessels; (2) the concentration of respiratory compounds to be used and time-dependency of compound penetration; (3) injection strategies to be used; and (4) ways to normalize data between experimental groups. All these considerations have been examined in the current paper and are discussed in further detail below. These methods are presented as simplified approaches to generating consistent metabolic oxygen flux data using single 3D spheroids with the XFe96 Flux analyzer. This experimental approach can be used as a starting point and rubric for use in other spheroid models that are easily implemented within a basic laboratory setting.

Considerations

Spheroid growth, size, and sensitivity of XF technology

To establish reproducible data with XF technology, it is essential to characterize and optimize the assay for the specific model. This approach is relatively simple in a basic monolayer of cells; however, this presents additional challenges when cultivating cells as 3D spheroids. During the experiments presented here, RPMI medium from the manufacturer was supplemented upon use. While it is noted that some cell lines, namely HepG2/C3A, were cultured in DMEM growth medium, during these relatively short assays (~3–5 h), substitution with RPMI–DMEM formulations had limited impact on XF analysis. The formulation of the two media are very similar, and users could 'tune' Seahorse RPMI media to match the matrix of their cell culture mediums through supplementation, e.g., increased glucose, further addition of carbohydrate sources. Critical to the final formulation of all XF buffers and mediums is the absence of phenol-red, which is likely to interfere with the fluorescent probes within the XF probe cartridge plate, and sodium bicarbonate, which will lead to alkalinity due to the lack of CO_2 buffering present in cell culture incubators. Other media and buffers can be purchased and/or made in-house. For example, Krebs Ringer HEPES buffer is a simple buffer that can be used to assess respiration in many different cells, including spheroid models. However, users of XF assays should note that a change in medium/buffer and its supplementation may change its overall buffering capacity. This is of particular concern when users may be interested in measuring ECAR, in which the buffer factor of the medium needs to be assessed to allow ECAR transformation to proton efflux rate (PER).

As cellular OCR measured by XF technology is proportional to cell density when the cell number in the well is within the sensitivity of the system, it was important to investigate this relationship using single 3D spheroids. By probing OCR of single 3D spheroids cultured from 4 different cancer cell lines seeded at densities of 1,000, 2,000, 4,000, or 8,000 cells per well, we show that the XFe96 analyzer is sensitive enough to pick up changes in the rate of mitochondrial respiration

740   between 3D spheroids grown from different cell seeding densities (**Figure 3**). We show that the
741   optimal range of cell seeding density, and thus spheroid volume for forming 3D spheroids for
742   probing OCR, differ depending on cell type. This is shown by the linear relationship between OCR
743   and seeding density or spheroid volume (**Figure 3**). For A549 and HepG2/C3A cells, the optimal
744   seeding density for OCR sensitivity was between 1,000 and 8,000 cells/well; it was 2,000–8,000
745   cells/well for MCF-7 and 4,000–8,000 cells/well for SK-OV-3 cells. These data demonstrate that
746   optimization of spheroid size is of particular importance when assessing OCR using XF technology.

748   *Considerations on minimal and maximal spheroid volumes and basal OCR*
749   In general, there will always be minimum and maximum thresholds for measurable OCR
750   parameters recommended by the manufacture for these experiments. For the XFe96 analyzer,
751   basal OCR between 20 pmol O_2/min/well and 200 pmol O_2/min/well are the lower and upper
752   limits, respectively. This is the case with monolayer cells and spheroids, and where the
753   experimental model sits within this dynamic OCR range will depend on the amount of biological
754   material available, e.g., the number of cells as a monolayer or the size of spheroids. See **Table 4**
755   for an example of how OCR thresholds were achieved by the spheroid models used here. It may
756   be prudent to check the oxygen level within the well for which these data are also available from
757   these measurements as the level data. This should be viewed routinely from each experiment for
758   quality control purposes. If there is oxygen depletion in the well, this will be made evident within
759   the data. Should this be the case, adjusting the measurement cycles within the experiment may
760   be necessary; for example, increasing the mixing step such that the oxygen level in the well is
761   recovered before the next measurement period within the measurement cycle. Though possible,
762   we have found this to be very unlikely for single-spheroid experiments using the cell lines
763   described.

765   *Choice of mitochondrial uncouplers for extracellular flux assays*
766   Proton ionophores, such as carbonyl cyanide 4-(trifluoromethoxy) phenylhydrazone (FCCP)[21],
767   carbonyl cyanide m-chlorophenyl hydrazone (CCCP)[22] or BAM15[23], are potent small-molecule
768   chemicals capable of disrupting the electrochemical proton gradient across mitochondrial
769   membranes, inhibiting the production of ATP, and ultimately uncoupling mitochondrial
770   respiration[24]. New small molecules continue to be developed for these purposes, particularly in
771   the treatment of metabolic disease[25-27]; refer to two excellent reviews[28,29]. Conversely,
772   uncoupling of oxidative respiration has been linked with undesirable off-target toxicity[30].
773   However, within *in vitro* cellular assays, the molecule FCCP depolarizes mitochondrial membrane
774   potential and exerts off-target effects such as plasma membrane depolarization, disrupting NA^+
775   ion flux[31]; interference with cellular protein processing[32], and even inducing cellular
776   senescence[33]. BAM15 was originally introduced in 2013 as a mitochondrial uncoupler with
777   minimal influence on plasma membranes[23], with protonophoric activity in the micromolar range
778   in whole cells and nanomolar range in isolated mitochondria[23,34].

780   Given the potency of FCCP on plasma membrane depolarization, BAM15 is a more reliable
781   protonophore for uncoupling respiration in intact whole cells in extracellular flux assays.
782   Although FCCP and its counterpart, CCCP, have been used for over 50 years to assay maximal
783   respiratory capacities and continue to be used widely in XF studies, the use of these small

784 molecules often underestimates mitochondrial and cellular metabolic capacity. This is partly
785 linked to why so many publications using XF technology fall into the trap of reporting negative
786 spare respiratory capacities or underestimate true mitochondrial respiratory capacities when
787 FCCP is used. The added potency of FCCP in intact cells and tissues often leads to compromised
788 mitochondrial function, and cells can struggle to operate appropriately to sustain a maximum
789 respiratory capacity across multiple measurement cycles following their addition, even at very
790 low concentrations[35]. Therefore, the response of cells to FCCP can be found in many studies to
791 drop off following the initial measurement cycle period. While FCCP has been routinely used for
792 XF analysis, BAM15 is used preferentially in cases involving whole cells or spheroid models, given
793 that it can maintain a maximum respiratory capacity in fully depolarized mitochondria at
794 concentrations as high as 10 μM [3]. Moreover, BAM15 induces effects on extracellular
795 acidification, which coincides with that of nutrient oxidation through the hydration of CO_2 to form
796 HCO_3^- and H^+ to a greater extent than FCCP[3]. Nevertheless, in the case of isolated mitochondria
797 and permeabilized cells, any of these uncouplers should perform as well as BAM15 for
798 mitochondrial uncoupling if titrated at the correct concentration.
799
800 *Kinetics of compound penetration and assay cycling*
801 The concentrations, penetration, and kinetic profiles of chemical compounds used to conduct a
802 typical **MitoStress test** with 3D spheroids using the XF analyzer are more complex to address.
803 Given that spheroids present 3D structure, the penetration of molecules across the diameter of
804 the spheroid is an infinitely more complex process than across cell monolayers. For example, the
805 kinetic penetration and, therefore, sensitivity to the chemotherapeutic sorafenib was
806 determined by spheroid age and, therefore, size in a HepG2 spheroid model[36]. The ability of
807 small-molecule chemicals (e.g., drugs, nanoparticles) to reach a biological target depends on
808 several underlying factors, including the complexity of the system to be dynamically penetrated
809 and diffused through[37,38]. This is particularly true for drugs targeting tumor tissue[39]. Similar to
810 tumor targeting in the context of a 3D spheroid, size, compactness, and other phenotypic
811 responses such as the expression of drug transporter proteins can govern the penetration time
812 and concentration of a compound required to elicit a biological response.
813
814 In this protocol, we addressed the issue around penetration time and small-molecule
815 concentration in response to the ATP synthase inhibitor oligomycin, the protonophore and
816 mitochondrial uncoupler BAM15, and the combination of the Complex I and Complex III inhibitors
817 rotenone and antimycin A. By probing the OCR of single MCF-7 spheroids exposed to multiple
818 titrations of these common respiratory compounds, we demonstrate that the optimal
819 concentration of each compound required to induce a steady-state respiratory rate falls within a
820 similar range to that of monolayer cells (**Figure 4**). Importantly, and differing from their
821 monolayer counterparts, it is shown that increasing the number of measurement cycles between
822 injections is key to achieving a steady-state OCR in single 3D spheroids. These data highlight the
823 importance of compound penetration and their respective kinetic profiles when exploring
824 mitochondrial respiratory parameters of 3D spheroids using these approaches. Using spheroid
825 optimization properties, concentrations of compounds, and measurement cycle times informed
826 by the data presented in **Figure 3**, **Figure 4**, and **Figure 5**, a validated **MitoStress test** was
827 established for probing specific parameters of mitochondrial oxidative metabolism in a range of

828 cancer-derived 3D spheroids (**Figure 6**). Of importance, and like some monolayer cancer cell
829 lines[40], the maximal respiratory capacity (rate of uncoupled-stimulated respiration) of certain
830 cancer-derived 3D spheroids was inhibited by oligomycin (**Figure 5**). Specifically, 3D spheroids
831 grown from either A549 or MCF-7 cells showed a significantly lower maximal rate of respiration
832 when uncoupled with BAM15 following oligomycin injection compared to being uncoupled by
833 BAM15 without oligomycin (**Figure 5F** and **Figure 5H**). Given that this effect may be present
834 within other 3D spheroid cultures, we suggest that unless a previously validated protocol is
835 employed, maximal respiratory capacity in 3D spheroids should be estimated without oligomycin.
836
837 _Simultaneous collection of ECAR data as a measure of glycolytic flux in cellular spheroids_
838 As typically seen in the literature or information from the technology manufacturer, the glycolytic
839 rate of spheroids, measured as ECAR, is a secondary parameter that can be captured alongside
840 OCR. Calculating ECAR alone is not a useful or meaningful parameter in any XF experiment as it
841 is not corrected for the buffering capacity of the XF assay buffer or the addition of mitochondrial
842 acidification, which arises from the hydration of CO_2 to HCO_3^- and H^+. ECAR is only insightful once
843 these data corrections are applied, after which it becomes possible to provide more accurate
844 conclusions about glycolytic flux. To correct for the buffering capacity to generate more
845 meaningful PER data, one must know the volume of the microchamber for the spheroid
846 microplate. The manufacturer has been unable to provide a true volume for this with the
847 spheroid microplate, and therefore, PER data cannot be determined easily. Indeed, although
848 these measurements could be achieved empirically, this was beyond the scope of this
849 manuscript. However, with the appropriate corrections and knowing the volume of the
850 microchamber for a given spheroid size present (e.g., obtaining a measure of spheroid density)
851 in the well, ECAR data would become meaningful, and calculations of glycolytic PER could be
852 made. Hence, XF data could then be more informative for investigating glycolytic and oxidative
853 metabolism in spheroids, but only if these parameters were considered in depth.
854
855 _Spheroid formation, handling, transfer, and movement_
856 Some cell lines are better suited to the formation of spheroids than others and may not form
857 spheroids at all, e.g., MCF-7 ovarian cancer cells[41,42] form highly circular spheroids compared to
858 other cell lines (**Figure 3**). As another example, Capan-1 pancreatic cancer cells have been shown
859 to form better spheroids than Panc-1 or BxPC3[43]. Similarly, hepatic carcinoma cell lines are known
860 to have variable abilities to form compact spheroids[5,44], with an observed change in phenotype
861 such as enhanced drug metabolism or the production of albumin, as is the case for HepG2 versus
862 HepG2/C3A[9,45,46] or HepaRG spheroids[17,47,48]. Therefore, users should optimize spheroid culturing
863 techniques accordingly and perform titration experiments to determine optimal seeding density
864 and cultivation time course. In addition, the formulation and composition of assay media have
865 been shown to impact spheroid formulation, including the addition of methylcellulose, often
866 added to media to increase matrix viscosity[43,49,50]. Hence, the optimal cell medium composition
867 should be determined empirically for all cell lines used.
868
869 The number of medium exchanges throughout spheroid culture is determined by the cell line
870 used. However, typically, half-volume medium exchanges every 2–3 days is applicable in most
871 cases to replenish nutrients. We used the forced-aggregate approach to generate 3D spheroids

872 using cell-repellent microplates from commercially available sources for rapid development and
873 deployment of spheroid models in XF analyses studies. However, alternative platforms may be
874 better suited to generate spheroids from other cell types, e.g., hanging-drop or matrix-embedded
875 approaches. In resource-limited laboratories, users may wish to look toward the agarose–liquid
876 overlay technique for the formation of cell-repellent microplate surfaces[51,52] to significantly
877 reduce the economic costs of initial spheroid method development steps. The movement of
878 spheroids between culture vessels is necessary to perform XF analysis and other downstream
879 assays. Ease of transfer is typically dictated by spheroid size and overall density. We recommend
880 using a P200 or P1000 wide-orifice pipette tip to maintain spheroid integrity; smaller-bore
881 pipette tips risk mechanical disruption of the spheroid, which can be bought sourced
882 commercially or, with care, made by simply trimming the end of the pipette tip to increase the
883 orifice. However, this approach may be liable to introduce furring to the plastic around the end
884 of the tip, which could cause mechanical disruption during handling. The use of a backlight or
885 lightbox is also useful for spheroid handling and observation under a dissection microscope as an
886 essential step to ensure the successful transfer of spheroids into the spheroid assay microplate.
887 Moreover, the spheroid position within the well of a spheroid assay microplate is of particular
888 importance and directly impacts OCR and compound effect during a typical **MitoStress test**
889 (**Figure 7**), most likely due to the relationship of the spheroid position and the sensor probe
890 fluorophores.
891
892 *Background correction and temperature control wells*
893 The use of microplate-based assays is a widely used approach in several research areas; however,
894 their use presents several practical challenges. As is true in other experimental approaches,
895 particularly those that use the 96 (or greater) array format, microplate geometry and positioning
896 can influence temperature and gas-exchange gradients across the plate over time, often referred
897 to as 'edge effects'[53,54]. We found the same to be true of the spheroid assay microplate. Under
898 the manufacturer's guidelines and protocols, the outermost corner wells: A1, A12, H1, and H12
899 are always designated as background correction and temperature control wells for the XFe96
900 analyzer. Conversely, with the 24-well array format, A1 and D6 are designated as control wells,
901 alongside two other wells evenly spread across the middle of the plate at B4 and C3. On
902 performing XF spheroid analysis, we found significant deviation in data initially collected using
903 the manufacturer's guidance. This was despite the inclusion of the necessary steps to ensure
904 assay preequilibration to temperature and CO_2 content prior to commencing the acquisition of
905 data, often yielding negative values for OCR following the injection of certain respiratory
906 inhibitors (**Figure 8**).
907
908 We found these observations likely to be due to edge effects across the spheroid assay
909 microplate. In **Figure 8**, we found that redistributing background control wells across the
910 microplate, XF data were adjusted approximately 2-fold. Two most likely reasons are (1) due to
911 evaporation effects at the edge wells resulting in a smaller total volume chamber for the XFe96
912 probe to sample from, and (2) from inadequate temperature equilibrations between those wells
913 designated for background correction and sample wells, resulting in datasets that either mask or
914 over-inflate OCR. To avoid such outcomes, it is therefore recommended, especially within the
915 context of spheroid analysis, that users redistribute wells designated for background correction

916   across the entirety of the spheroid assay microplate and take necessary steps to pre-equilibrate
917   their assay prior to acquiring XF data.
918

919   _Normalization of data_
920   In addition to providing a detailed protocol for probing mitochondrial energy metabolism of
921   single 3D spheroids with XF technology, this paper also presents possible ways to normalize
922   mitochondrial respiratory rate data obtained with 3D spheroids. Using respiratory rate data
923   obtained with MCF-7 spheroids cultured at different cell seeding densities (**Figure 3**), we present
924   basal mitochondrial respiratory rates from MCF-7 spheroids of increasing size and diameter when
925   normalized to initial cell seeding density, spheroid volume, and dsDNA content (**Figure 9**). The
926   appropriate normalization method is paramount for the accurate interpretation of XF datasets,
927   particularly when comparing _in vitro_ 3D spheroid models and different cell types. Poor
928   normalization can lead to erroneous results that simply cannot be compared between datasets.
929   Protein content is not preferred for normalization of spheroid XF data, as pretreatments may
930   impact rates of protein synthesis without significant effect on respiratory rate. Moreover,
931   significant, inconsistent amounts of protein can bind to spheroid microplates upon cell lysis,
932   introducing variation in protein content between wells. This may be further complicated in XF
933   analyses using spheroids or nonadherent cells that require biomolecular glues to bind to, which
934   may contain protein.
935

936   Contrary to intracellular protein content, nuclear DNA content is independent of cell type and is
937   proportional to cell number (**Figure 9D**)—a more accurate and less time-consuming approach
938   than the disaggregation of spheroids for cell number quantification. Conversely, Yepéz et al.[55],
939   conducting XF analyses in monolayers of fibroblasts cells, found that normalizing XF data to cell
940   number introduced greater dispersion of data than before normalization. Nuclear DNA content
941   is independent of differentiated state or phenotype and hence is more accurate for the
942   normalization of spheroid data in XF assays than protein content. DNA content has also been a
943   proven strategy for the analysis of other metabolism-linked datasets[56]. However, it is important
944   to note that nuclear DNA content is quantified from all cells present within the spheroid;
945   therefore, normalization to DNA content is not recommended for XF datasets wherein spheroids
946   undergo treatments that may result in significant loss of cell viability. For such datasets, if
947   feasible, normalization to cell viability is preferred, or the data can be baseline-corrected to basal
948   respiration.
949

950   _Using spare respiratory capacity as an exemplar for the importance of data normalization_
951   Spare respiratory capacity is a measure of the rate of maximal mitochondrial respiratory capacity
952   minus basal mitochondrial respiratory rate (**Figure 6**). However, the issue with reporting data of
953   this type as a rate, i.e., $pmolO_2$/min/well within certain experiments, is that the data are void of
954   normalization. Even if one normalizes spheroid data to cell density/DNA content, this often
955   excludes the key parameter that needs to be normalized for—mitochondrial density within the
956   cells. Given that a change in mitochondrial density will lead to a proportional change in basal and
957   maximal respiration, spare capacity will also increase. For example, if spheroid OCR_{basal} is 200 and
958   OCR_{max} is 400, spare capacity is reported as 200; if OCR_{basal} is 100 and OCR_{max}, then spare capacity
959   is also 100; however, as a percentage, they are both 50% of maximal (or 100% of basal).

Therefore, the spare capacity is not changed between these two examples, despite differences in rates of 200 and 100 when calculated as pmols O_2/min/well. Internally normalized values are more reliable and insightful to make XF data more comparable across studies and projects. To do this for spare respiratory capacity, we have chosen to present this as a percentage of maximal respiration instead of an absolute rate. This could also be presented as a percentage of basal respiration. This would be the case if working with cells or spheroids. However, given that the location of the spheroid in the microwell plate may alter the absolute OCR but not the relative changes with inhibitors or uncouplers, it is more important to look at internally normalized responses in spheroids as fold change or percentages.

The spheroid models generated here present a range of cell types and architecture that cannot be captured in classical 2D models. These include heterogeneous, spatial arrangement of cells in three dimensions, enhanced cell–cell contacts (e.g., formation of gap junctions and extracellular matrices), and biochemical gradients across the spheroid diameter (e.g., pH gradients, oxygen diffusion access to nutrients). Using extracellular flux to study *in vitro* spheroid biology could allow optimal targets for drug therapies to be identified through metabolic perturbation observations. These could be extrapolated from *in vitro* spheroids to *in vivo* tumors and identify pathways that may target spheroid-tumor metabolism, e.g., carbohydrate utilization during spheroid growth. Therapeutic modalities may be effective in targeting spheroids in early growth phases but prove less effective in the later phases of spheroid growth as metabolic network complexity matures. To conclude, the development of 3D cell culture models and sophisticated analysis technologies in biological research will continue to be a dynamic and rapidly changing field with unsurpassed potential. Extracellular flux analysis of *in vitro* cell culture spheroids could be employed as a cutting-edge research method to advance research outcomes that could be extrapolated to understand human-relevant biology better, reduce the use of animal models in research, and enhance patient-centric research.

DISCLOSURES:
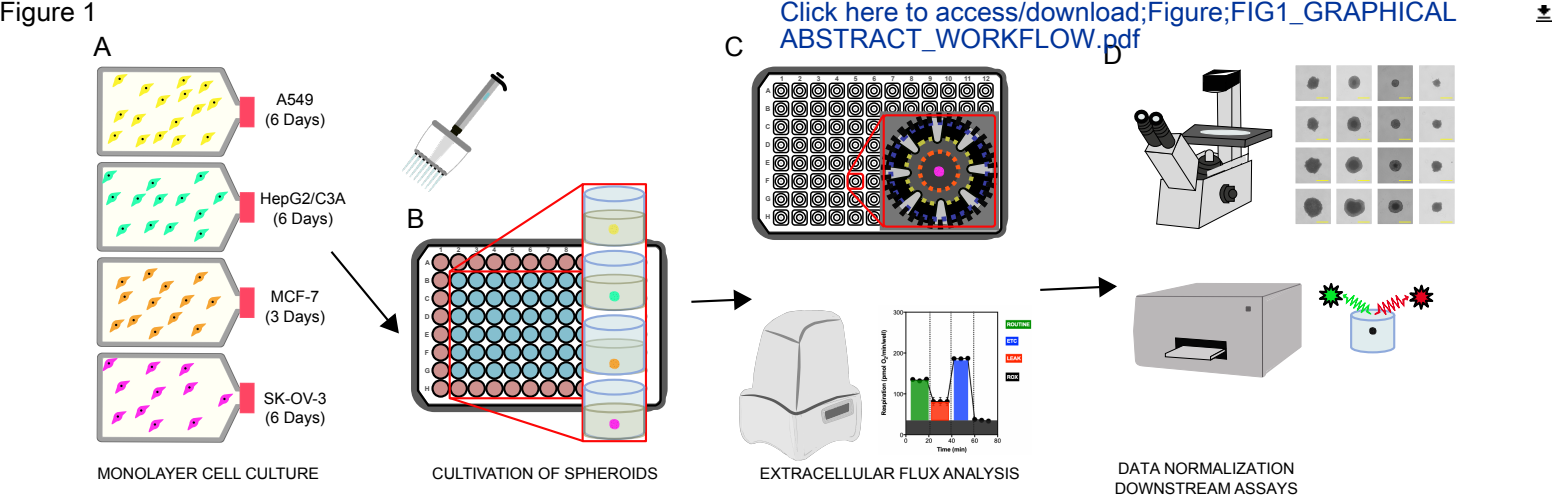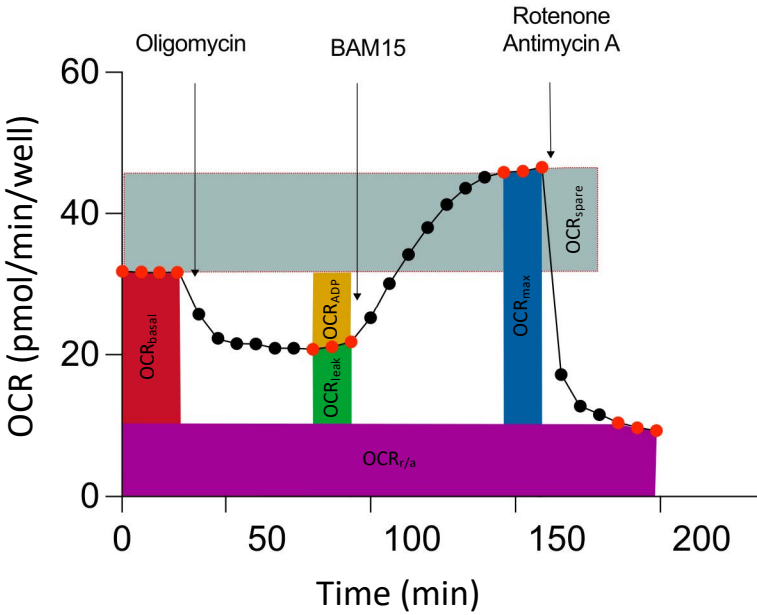The authors have no conflicts of interest to declare.

REFERENCES:
1   Correa de Sampaio, P. et al. A heterogeneous in vitro three dimensional model of tumour-stroma interactions regulating sprouting angiogenesis. *PLoS One.* **7** (2), e30753 (2012).
2   Amann, A. et al. Development of an innovative 3D cell culture system to study tumour-stroma interactions in non-small cell lung cancer cells. *PLoS One.* **9** (3), e92511 (2014).
3   Russell, S., Wojtkowiak, J., Neilson, A., Gillies, R. J. Metabolic profiling of healthy and cancerous tissues in 2D and 3D. *Scientific Reports.* **7** (1), 15285 (2017).
4   Zanoni, M. et al. 3D tumor spheroid models for in vitro therapeutic screening: a systematic approach to enhance the biological relevance of data obtained. *Scientific Reports.* **6** 19103 (2016).

1004 5   Song, Y. et al. Patient-derived multicellular tumor spheroids towards optimized treatment
1005 for patients with hepatocellular carcinoma. *Journal of Experimental and Clinica Cancer Research.*
1006 **37** (1), 109 (2018).
1007 6   Courau, T. et al. Cocultures of human colorectal tumor spheroids with immune cells reveal
1008 the therapeutic potential of MICA/B and NKG2A targeting for cancer treatment. *Journal for*
1009 *ImmunoTherapy of Cancer.* **7** (1), 74 (2019).
1010 7   Ivanova, E. et al. Use of ex vivo patient-derived tumor organotypic spheroids to identify
1011 combination therapies for HER2 mutant non-small cell lung cancer. *Clinical Cancer Research.* **26**
1012 (10), 2393–2403 (2020).
1013 8   Mandon, M., Huet, S., Dubreil, E., Fessard, V., Le Hegarat, L. Three-dimensional HepaRG
1014 spheroids as a liver model to study human genotoxicity in vitro with the single cell gel
1015 electrophoresis assay. *Scientific Reports.* **9** (1), 10548 (2019).
1016 9   Stampar, M. et al. Hepatocellular carcinoma (HepG2/C3A) cell-based 3D model for
1017 genotoxicity testing of chemicals. *Science of the Total Environment.* **755** (Pt 2), 143255 (2020).
1018 10   Coltman, N. J. et al. Application of HepG2/C3A liver spheroids as a model system for
1019 genotoxicity studies. *Toxicology Letters.* **345**, 34–45 (2021).
1020 11   Tchoryk, A. et al. Penetration and uptake of nanoparticles in 3D tumor spheroids.
1021 *Bioconjugate Chemistry.* **30** (5), 1371–1384 (2019).
1022 12   Leite, P. E. C. et al. Suitability of 3D human brain spheroid models to distinguish toxic
1023 effects of gold and poly-lactic acid nanoparticles to assess biocompatibility for brain drug
1024 delivery. *Partical Fibre Toxicology.* **16** (1), 22 (2019).
1025 13   Elje, E. et al. Hepato(Geno)toxicity assessment of nanoparticles in a HepG2 liver spheroid
1026 model. *Nanomaterials.* **10** (3), 545 (2020).
1027 14   Conway, G. E. et al. Adaptation of the in vitro micronucleus assay for genotoxicity testing
1028 using 3D liver models supporting longer-term exposure durations. *Mutagenesis.* **35** (4), 319–330
1029 (2020).
1030 15   Wang, Z. et al. HepaRG culture in tethered spheroids as an in vitro three-dimensional
1031 model for drug safety screening. *Journal of Applied Toxicology.* **35** (8), 909–917 (2015).
1032 16   Proctor, W. R. et al. Utility of spherical human liver microtissues for prediction of clinical
1033 drug-induced liver injury. *Archives of Toxicology.* **91** (8), 2849–2863 (2017).
1034 17   Basharat, A., Rollison, H. E., Williams, D. P., Ivanov, D. P. HepG2 (C3A) spheroids show
1035 higher sensitivity compared to HepaRG spheroids for drug-induced liver injury (DILI). *Toxicology*
1036 *and Applied Pharmacology.* **408**, 115279 (2020).
1037 18   Benning, L., Peintner, A., Finkenzeller, G., Peintner, L. Automated spheroid generation,
1038 drug application and efficacy screening using a deep learning classification: a feasibility study.
1039 *Scientific Reports.* **10** (1), 11071 (2020).
1040 19   Mittler, F. et al. High-content monitoring of drug effects in a 3D spheroid model. *Frontiers*
1041 *in Oncology.* **7,** 293 (2017).
1042 20   Brand, M. D., Nicholls, D. G. Assessing mitochondrial dysfunction in cells. *The Biochemical*
1043 *Journal.* **435** (2), 297–312 (2011).
1044 21   Benz, R., McLaughlin, S. The molecular mechanism of action of the proton ionophore FCCP
1045 (carbonylcyanide p-trifluoromethoxyphenylhydrazone). *Biophysical Journal.* **41** (3), 381–398
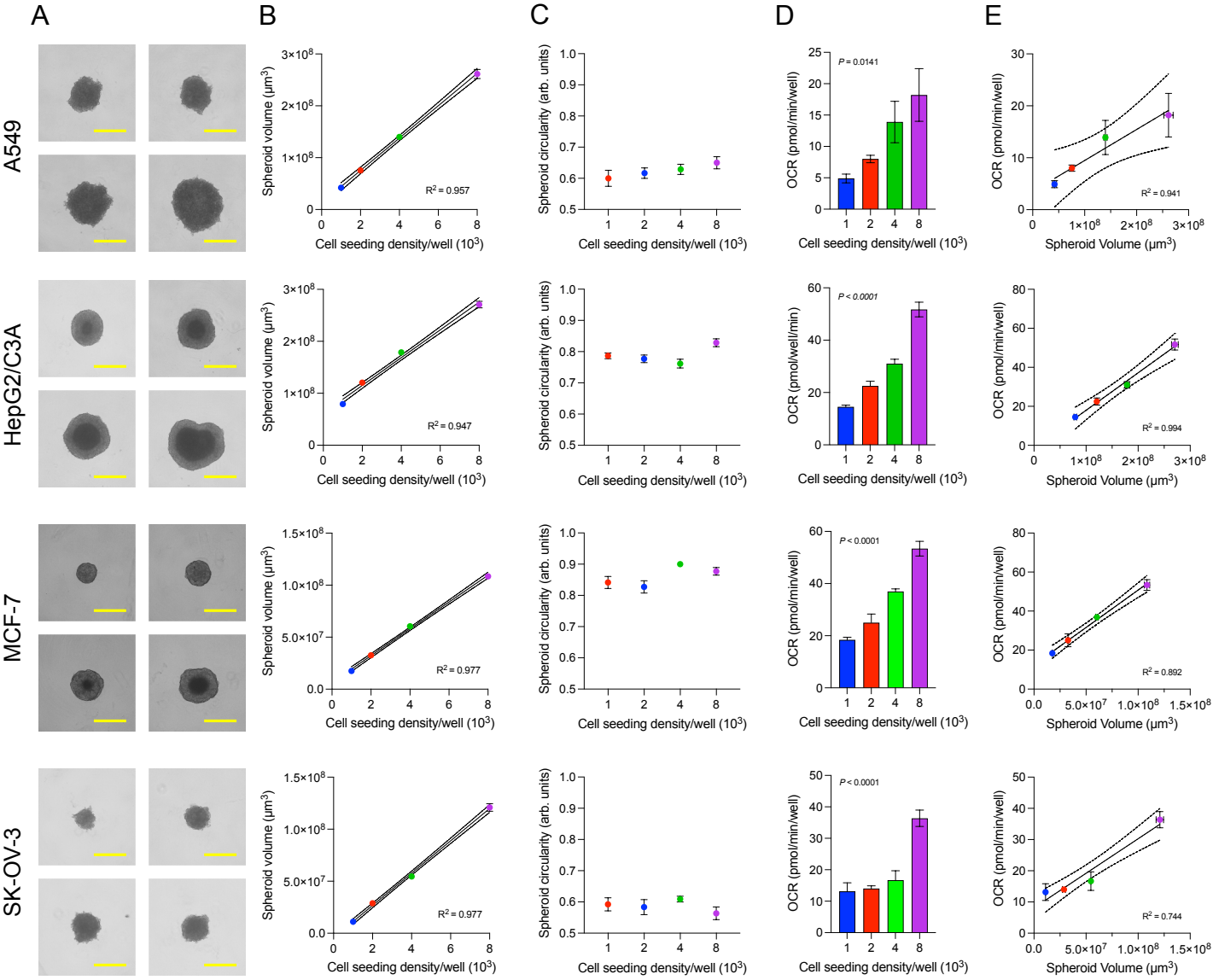1046 (1983).

1047   22   Kasianowicz, J., Benz, R., McLaughlin, S. The kinetic mechanism by which CCCP (carbonyl
1048   cyanide m-chlorophenylhydrazone) transports protons across membranes. *The Journal of*
1049   *Membrane Biology.* **82** (2), 179–190 (1984).

1050   23   Kenwood, B. M. et al. Identification of a novel mitochondrial uncoupler that does not
1051   depolarize the plasma membrane. *Molecular Metabolism.* **3** (2), 114–123 (2013).

1052   24   Mitchell, P. Coupling of phosphorylation to electron and hydrogen transfer by a chemi-
1053   osmotic type of mechanism. *Nature.* **191**, 144–148 (1961).

1054   25   Alexopoulos, S. J. et al. Mitochondrial uncoupler BAM15 reverses diet-induced obesity
1055   and insulin resistance in mice. *Nature Communications.* **11** (1), 2397 (2020).

1056   26   Chen, S.-Y. et al. Mitochondrial uncoupler SHC517 reverses obesity in mice without
1057   affecting food intake. *Metabolism - Clinical and Experimental.* **117**, 154724 (2021).

1058   27   Goedeke, L., Shulman, G. I. Therapeutic potential of mitochondrial uncouplers for the
1059   treatment of metabolic associated fatty liver disease and NASH. *Molecular Metabolism.* **46**
1060   101178 (2021).

1061   28   Hill, B. G. et al. Integration of cellular bioenergetics with mitochondrial quality control and
1062   autophagy. *Biological chemistry.* **393** (12), 1485–1512 (2012).

1063   29   Demine, S., Renard, P., Arnould, T. Mitochondrial uncoupling: a key controller of biological
1064   processes in physiology and diseases. *Cells.* **8** (8), 795 (2019).

1065   30   Wang, J. et al. Uncoupling effect of F16 is responsible for its mitochondrial toxicity and
1066   anticancer activity. *Toxicological Sciences.* **161** (2), 431–442 (2018).

1067   31   Tretter, L., Chinopoulos, C., Adam-Vizi, V. Plasma membrane depolarization and disturbed
1068   Na+ homeostasis induced by the protonophore carbonyl cyanide-p-trifluoromethoxyphenyl-
1069   hydrazon in isolated nerve terminals. *Molecular Pharmacology.* **53** (4), 734–741 (1998).

1070   32   Connop, B. P., Thies, R. L., Beyreuther, K., Ida, N., Reiner, P. B. Novel effects of FCCP
1071   [carbonyl cyanide p-(trifluoromethoxy) phenylhydrazone] on amyloid precursor protein
1072   processing. *Journal of neurochemistry.* **72** (4), 1457–1465 (1999).

1073   33   Stöckl, P. et al. Partial uncoupling of oxidative phosphorylation induces premature
1074   senescence in human fibroblasts and yeast mother cells. *Free Radical Biology and Medicine.* **43**
1075   (6), 947–958 (2007).

1076   34   Firsov, A. M. et al. Protonophoric action of BAM15 on planar bilayers, liposomes,
1077   mitochondria, bacteria and neurons. *Bioelectrochemistry.* **137**, 107673 (2021).

1078   35   Dranka, B. P., Hill, B. G., Darley-Usmar, V. M. Mitochondrial reserve capacity in endothelial
1079   cells: The impact of nitric oxide and reactive oxygen species. *Free Radical Biology and Medicine.*
1080   **48** (7), 905–914 (2010).

1081   36   Eilenberger, C., Rothbauer, M., Ehmoser, E. K., Ertl, P., Kupcu, S. Effect of spheroidal age
1082   on sorafenib diffusivity and toxicity in a 3D HepG2 spheroid model. *Scientific Reports.* **9** (1), 4863
1083   (2019).

1084   37   van den Brand, D., Veelken, C., Massuger, L., Brock, R. Penetration in 3D tumor spheroids
1085   and explants: Adding a further dimension to the structure-activity relationship of cell-penetrating
1086   peptides. *Biochimica et Biophysica Acta (BBA) - Biomembranes.* **1860** (6), 1342–1349 (2018).

1087   38   Niora, M. et al. Head-to-head comparison of the penetration efficiency of lipid-based
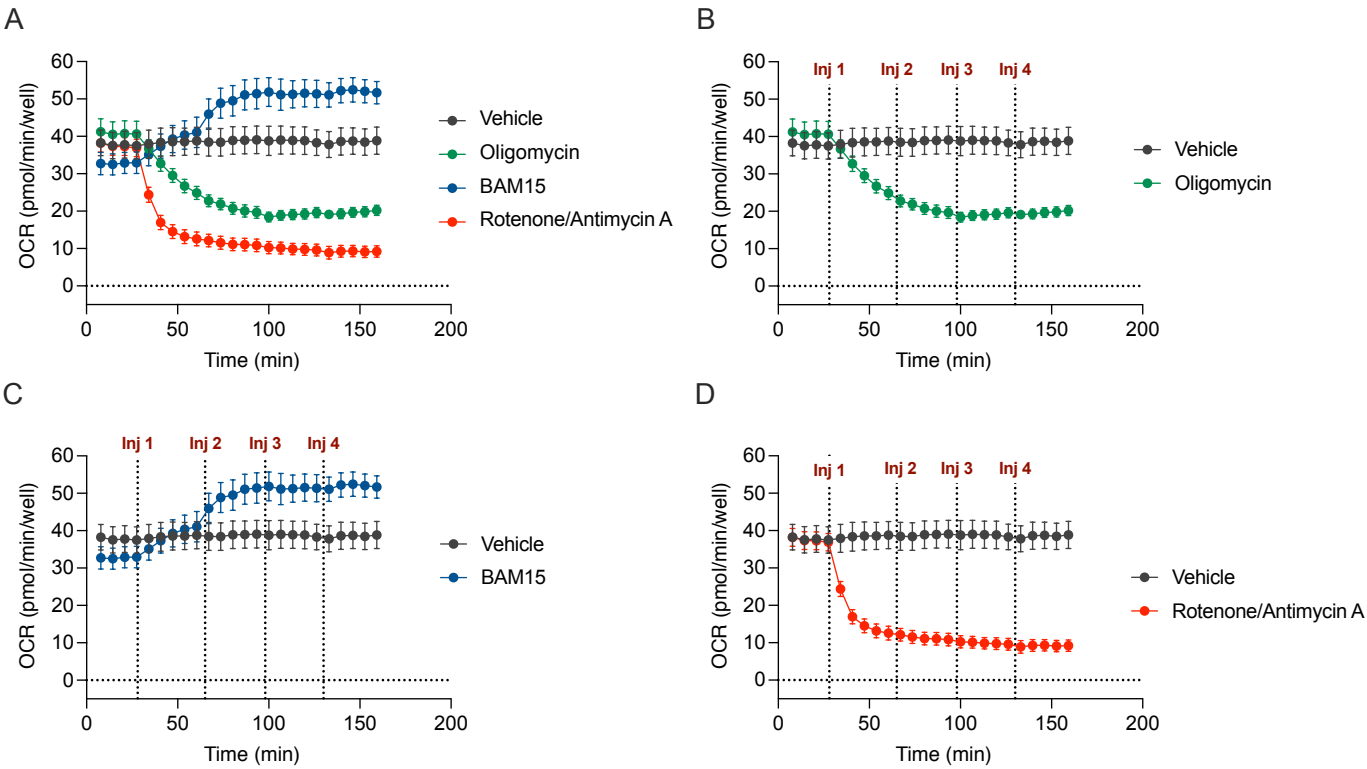1088   nanoparticles into tumor spheroids. *ACS Omega.* **5** (33), 21162–21171 (2020).

1089 39 Millard, M. et al. Drug delivery to solid tumors: the predictive value of the multicellular
1090 tumor spheroid model for nanomedicine screening. *International Journal of Nanomedicine.* **12**
1091 7993–8007 (2017).
1092 40 Ruas, J. S. et al. Underestimation of the maximal capacity of the mitochondrial electron
1093 transport system in oligomycin-treated cells. *PLoS One.* **11** (3), e0150967 (2016).
1094 41 Benton, G., DeGray, G., Kleinman, H. K., George, J., Arnaoutova, I. In vitro microtumors
1095 provide a physiologically predictive tool for breast cancer therapeutic screening. *PLoS One.* **10**
1096 (4), e0123312 (2015).
1097 42 Hirpara, J. et al. Metabolic reprogramming of oncogene-addicted cancer cells to OXPHOS
1098 as a mechanism of drug resistance. *Redox Biology.* **25**, 101076 (2019).
1099 43 Ware, M. J. et al. Generation of homogenous three-dimensional pancreatic cancer cell
1100 spheroids using an improved hanging drop technique. *Tissue Engineering. Part C, Methods.* **22**
1101 (4), 312–321 (2016).
1102 44 Song, Y. et al. TGF-β-independent CTGF induction regulates cell adhesion mediated drug
1103 resistance by increasing collagen I in HCC. *Oncotarget.* **8** (13), 21650–21662 (2017).
1104 45 Wrzesinski, K. et al. HepG2/C3A 3D spheroids exhibit stable physiological functionality for
1105 at least 24 days after recovering from trypsinisation. *Toxicology Research.* **2** (3), 163–172 (2013).
1106 46 Gaskell, H. et al. Characterization of a functional C3A liver spheroid model. *Toxicology*
1107 *Research.* **5** (4), 1053–1065 (2016).
1108 47 Takahashi, Y. et al. 3D spheroid cultures improve the metabolic gene expression profiles
1109 of HepaRG cells. *Bioscience Reports.* **35** (3), e00208 (2015).
1110 48 Hendriks, D. F. G., Puigvert, L. F., Messner, S., Mortiz, W., Ingelman-Sundberg, M. Hepatic
1111 3D spheroid models for the detection and study of compounds with cholestatic liability. *Scientific*
1112 *Reports.* **6**, 35434 (2016).
1113 49 Leung, B. M., Lesher-Perez, S. C., Matsuoka, T., Moraes, C., Takayama, S. Media additives
1114 to promote spheroid circularity and compactness in hanging drop platform. *Biomaterials Science.*
1115 **3** (2), 336–344 (2015).
1116 50 Cavo, M. et al. A synergic approach to enhance long-term culture and manipulation of
1117 MiaPaCa-2 pancreatic cancer spheroids. *Scientific Reports.* **10** (1), 10192 (2020).
1118 51 Carlsson, J., Yuhas, J. M. Liquid-overlay culture of cellular spheroids. *Recent Results in*
1119 *Cancer Research.* **95**, 1–23 (1984).
1120 52 Costa, E. C., Gaspar, V. M., Coutinho, P., Correia, I. J. Optimization of liquid overlay
1121 technique to formulate heterogenic 3D co-cultures models. *Biotechnology and Bioengineering.*
1122 **111** (8), 1672–1685 (2014).
1123 53 Lundholt, B. K., Scudder, K. M., Pagliaro, L. A simple technique for reducing edge effect in
1124 cell-based assays. *Journal of Biomolecular Screening.* **8** (5), 566–570 (2003).
1125 54 Zhang, X. D. et al. The use of strictly standardized mean difference for hit selection in
1126 primary RNA interference high-throughput screening experiments. *Journal of Biomolecular*
1127 *Screening.* **12** (4), 497–509 (2007).
1128 55 Yepez, V. A. et al. OCR-Stats: Robust estimation and statistical testing of mitochondrial
1129 respiration activities using Seahorse XF Analyzer. *PLoS One.* **13** (7), e0199938 (2018).
1130 56 Silva, L. P. et al. Measurement of DNA concentration as a normalization strategy for
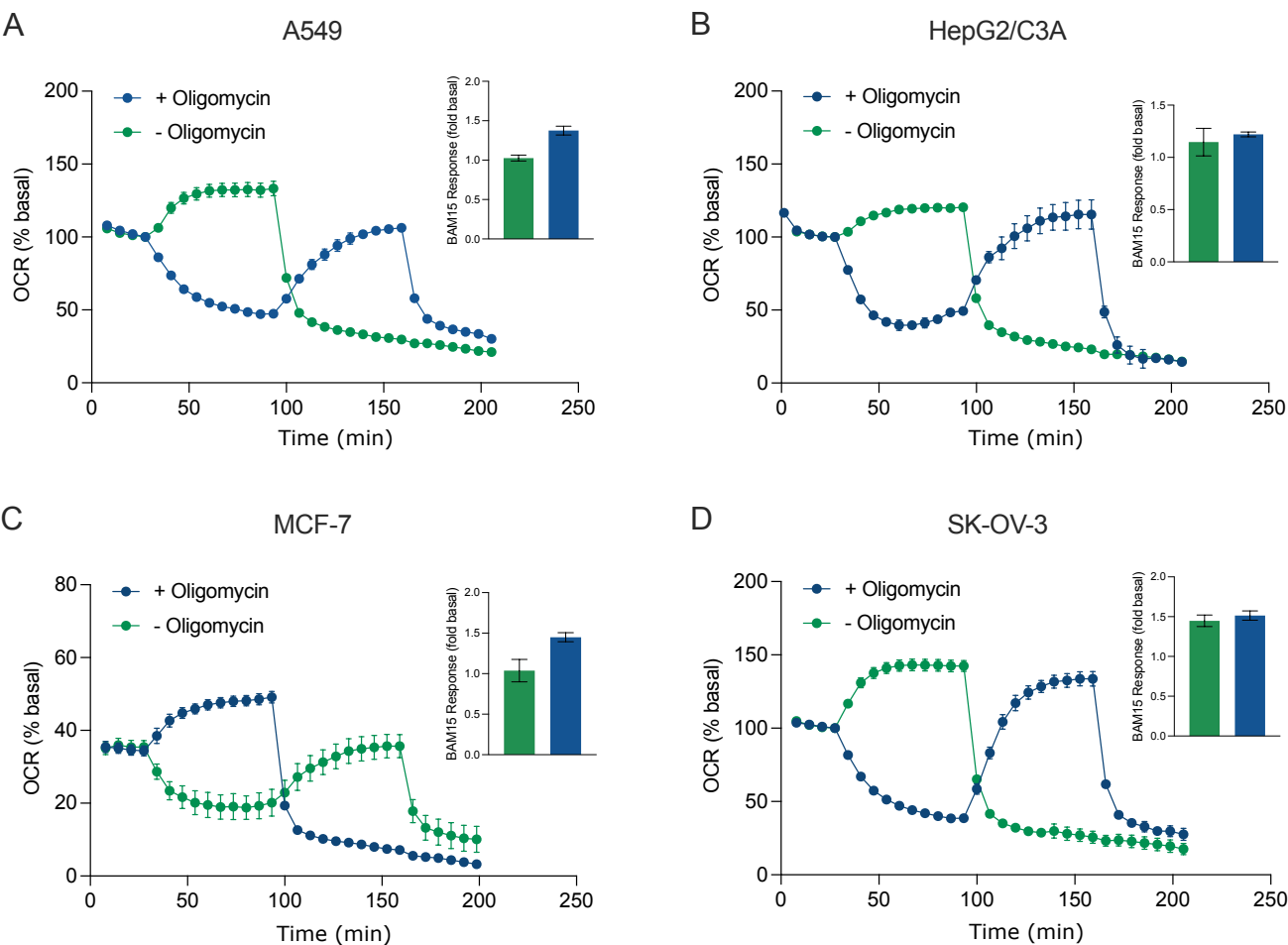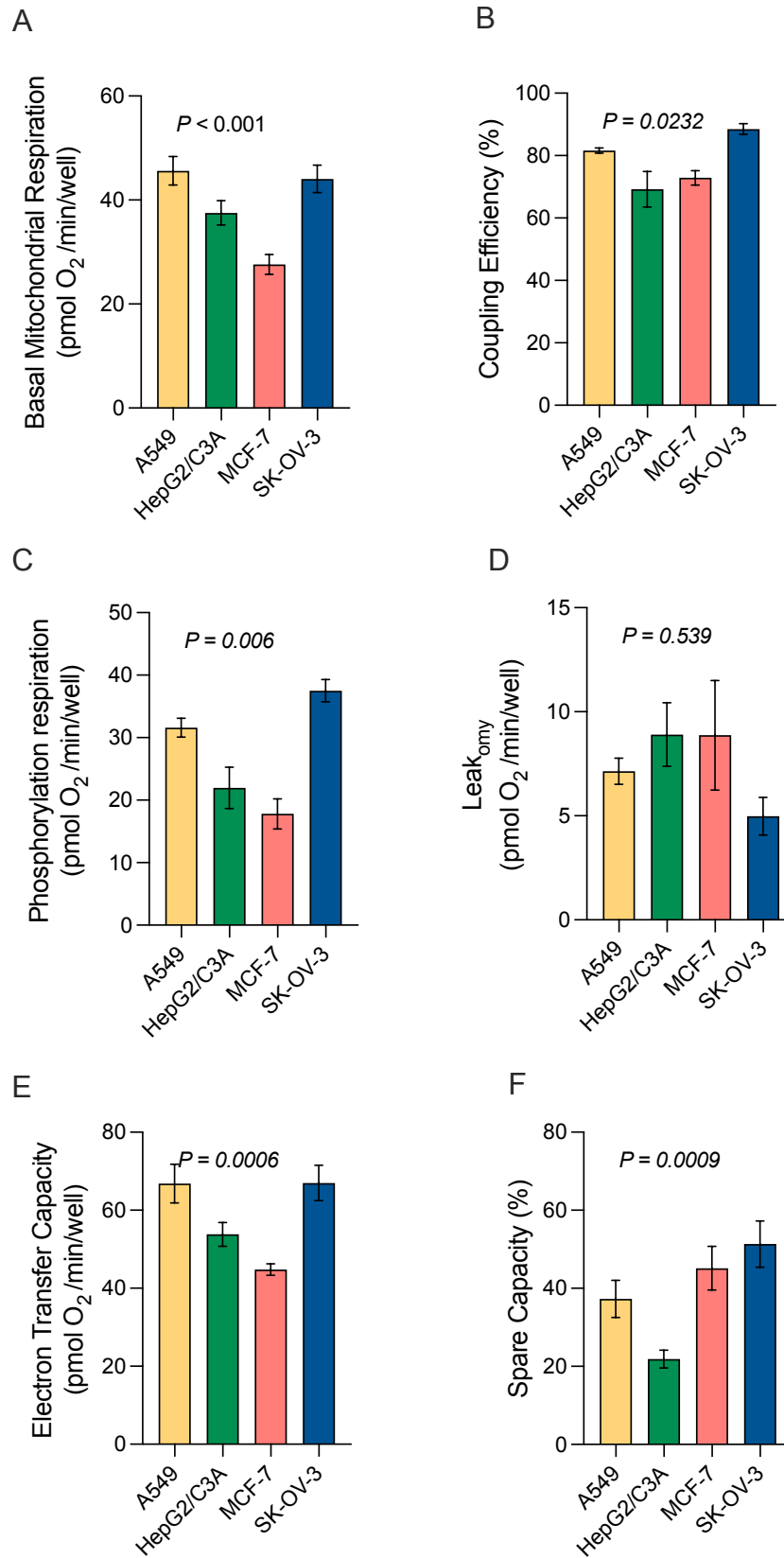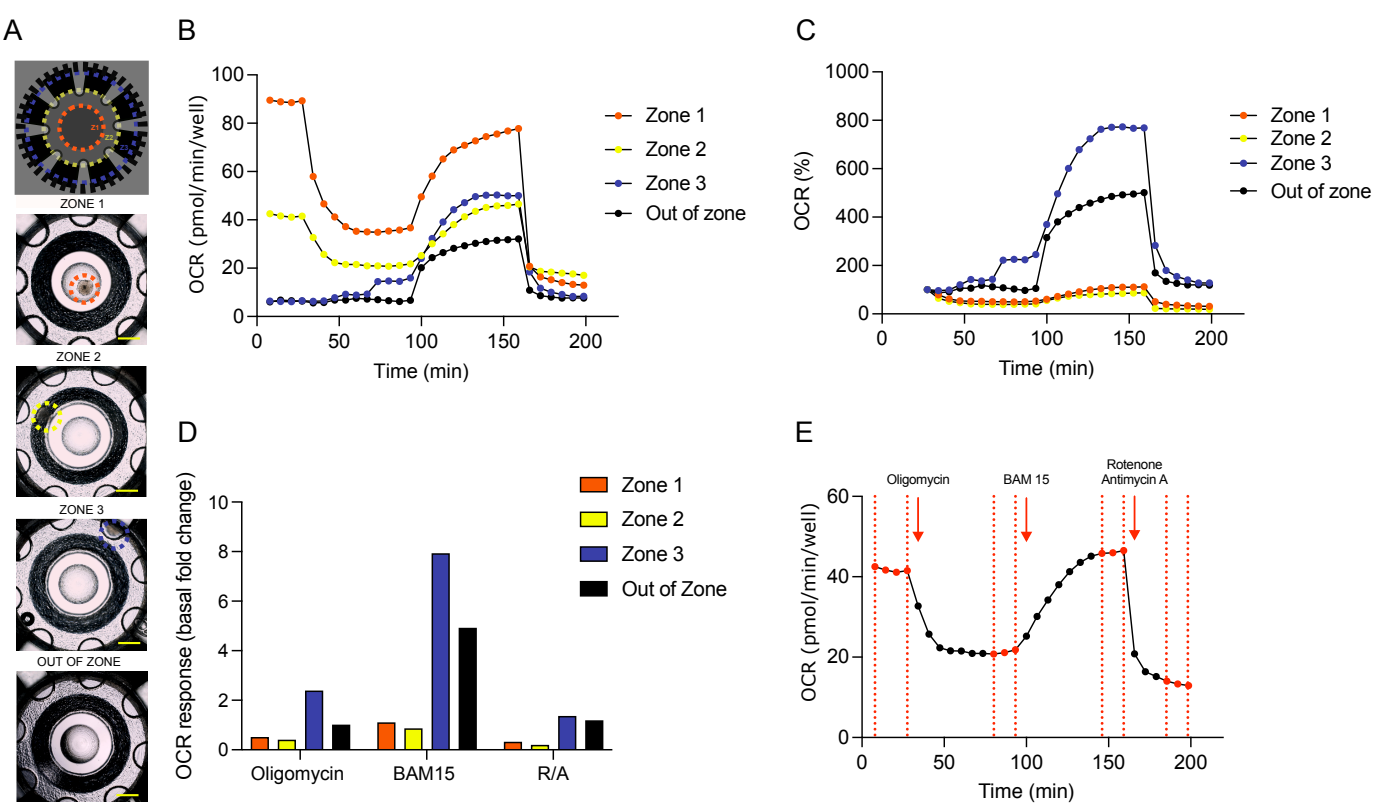1131 metabolomic data from adherent cell lines. *Analytical Chemistry.* **85** (20), 9536–9542 (2013).
1132

Figure 1

A

A549
(6 Days)

HepG2/C3A
(6 Days)

MCF-7
(3 Days)

SK-OV-3
(6 Days)

MONOLAYER CELL CULTURE

B

CULTIVATION OF SPHEROIDS

C

EXTRACELLULAR FLUX ANALYSIS

D

DATA NORMALIZATION
DOWNSTREAM ASSAYS

Figure 2

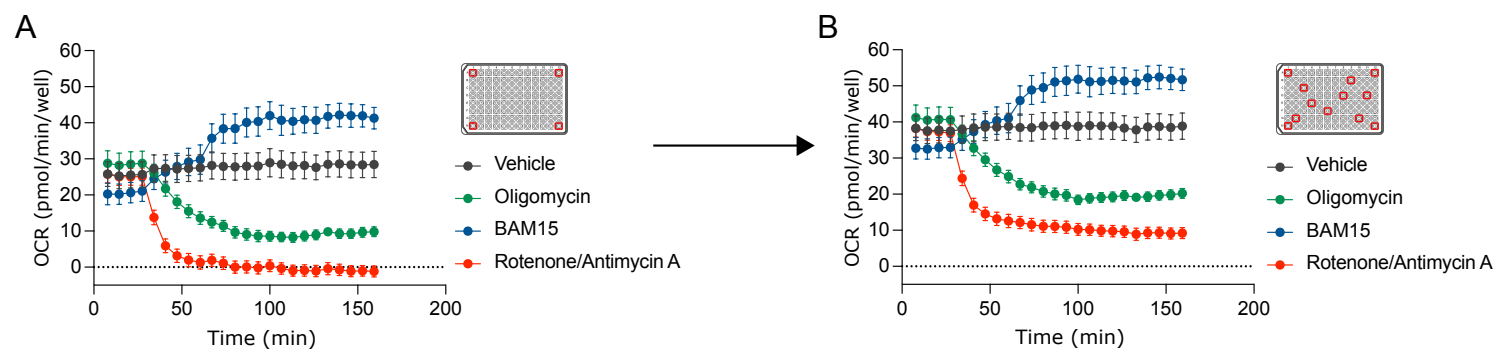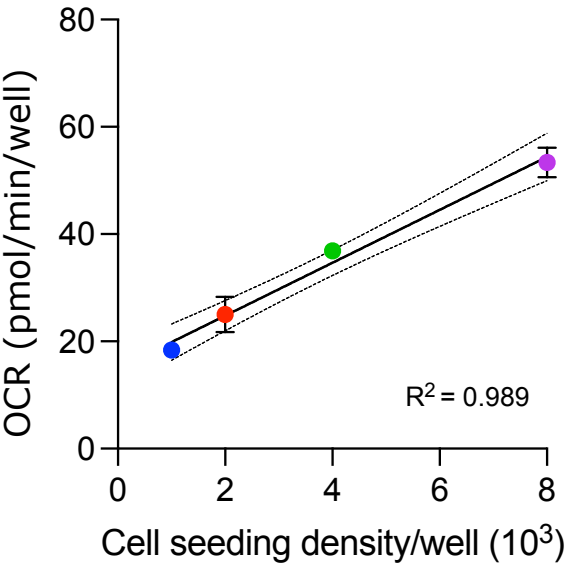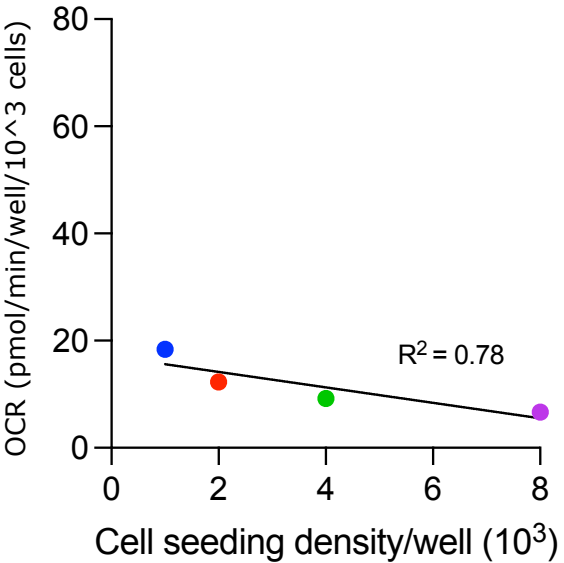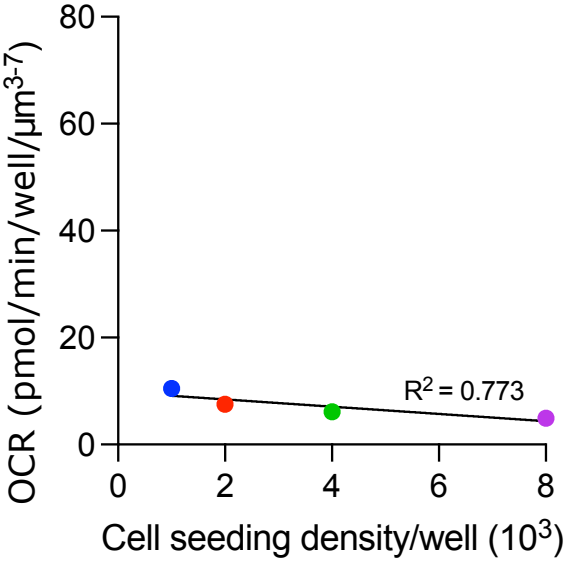| Parameter	Definition	Calculation
OCRbasal	Basal mitochondrial respiration is the amount of mitochondrial respiration required to meet the energetic demands of the biological model being measured assuming substrate availability to the cell is not limiting.	$OCR_{basal} = OCR - OCR_{r/a}$
OCRADP	ADP phosphorylation respiration is the proportion of basal mitochondrial respiration sensitive to oligomycin.	$OCR_{ADP} = OCR_{basal} - (OCR_{omy} - OCR_{r/a})$
OCRleak	Leak respiration is the proportion of basal mitochondrial respiration insensitive to oligomycin.	$OCR_{leak} = OCR_{omy} - OCR_{r/a}$
Coupling efficiency	Coupling efficiency of oxidative phosphorylation is the amount of respiration couple to ATP synthesis, approximated using OCR_{ADP} as a percentage of $OCR_{basal.}$	$(1- (OCR_{leak}/OCR_{basal})) \times 100$
OCRmax	Maximum respiratory capacity is a theoretical maximum rate of mitochondrial respiration that is achieved when phosphorylation control over energy demand is not rate limiting. This is measured by complete uncoupling and thus collapse of the proton gradient using protonophores such as BAM15, or FCCP.	$OCR_{max} = OCR_{BAM15} - OCR_{r/a}$
OCRspare	Spare respiratory capacity is a metabolic insurance policy of a cell and highlights a theoretical rate of respiration above OCR_{basal} that could be reached for surplus energy demand.	$OCR_{spare} = ((OCR_{max}/OCR_{basal}) -1) \times 100$
OCRr/a	Non-mitochondrial respiration is the oxygen consumption remaining in the absence of mitochondrial metabolism, achieved through the complete shutdown of the electron transport chain with inhibitors of respiratory complexes I and III (rotenone–antimycin A).	-

Figure 3

Figure 4

Figure 4

Figure 5

Figure 6

Figure 7

Figure 7

Figure 8

Figure 8

Figure 9

A

B

C

D
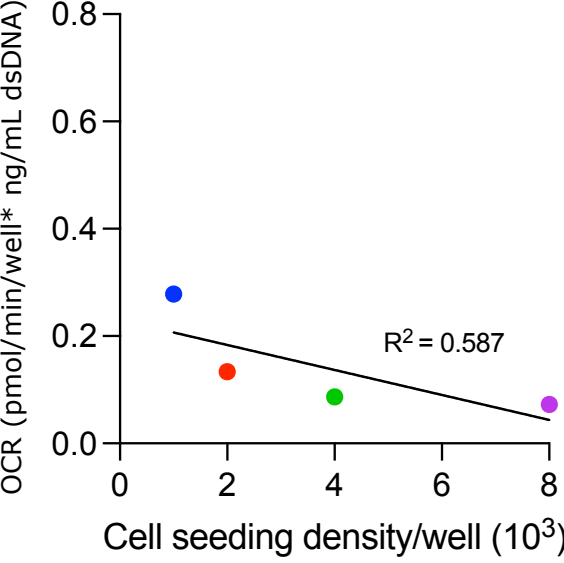
Table 1

Table 1

Cell line	Description	Culture medium	Source
A549	Lung carcinoma cell line	RPMI 1640 Sodium pyruvate (1 mM) Penicillin- Streptomycin - (100 U/mL – 100 mg/mL) 10 % (v/v) FBS	European Collection of Authenticated Cell Cultures (ECACC)
HepG2/C3A	Hepatic carcinoma cell line, a clonal derivative of the parent HepG2 cell line	DMEM Penicillin- Streptomycin - (100 U/mL – 100 mg/mL) 10 % (v/v) FBS	American Tissue Culture Collection (ATCC)
MCF7	Breast adenocarcinoma cell line	RPMI 1640 Sodium pyruvate (1 mM) Penicillin- Streptomycin - (100 U/mL – 100 mg/mL) 10 % (v/v) FBS	European Collection of Authenticated Cell Cultures (ECACC)
SK-OV-3	Ovarian adenocarcinoma cell line	RPMI 1640 Sodium pyruvate (1 mM) Penicillin- Streptomycin - (100 U/mL – 100 mg/mL) 10 % (v/v) FBS	European Collection of Authenticated Cell Cultures (ECACC)

Component	**RPMI assay medium (50 mL final volume)**
Base Medium	Agilent Seahorse XF RPMI, pH 7.4
Glucose (1 M sterile stock)	11 mM (0.55 mL stock solution)
L-glutamine (200 mM sterile stock)	2 mM (0.5 mL of stock solution)
Sodium pyruvate (100 mM sterile stock)	1 mM (0.5 mL of stock solution)

Table 2

Injection Strategy	Compound (Port)	XFe96 microwell starting volume (µL)	Desired final well concentration	Port Volume (µL)	Final XFe96 microwell volume post injection (µL)
	Oligomycin (A)	180	3 ug/mL	20	200
1	Rotenone (B)	200	2 µM	20	220
	Antimycin A (B)	200	2 µM	20	220
	BAM15 (A)	180	5 µM	20	200
2	Rotenone (B)	200	2 µM	20	220
	Antimycin A (B)	200	2 µM	20	220

Working stock concentration
30 µg/mL
22 µM
22 µM
50 µM
22 µM
22 µM

Table 3 Click here to access/download;Table;Table 3_rev (1).xlsx ⬇

Table 3.

Measurement Period	Injection Number and Port	Measurement Details	Period Duration (h:min:s)
Calibration	Not applicable	XF analysers always perform this calibration to make sure measurements are accurate	00:20:00 (this is an average and can vary between machines)
Equillibration	Not applicable	Equilibration occurs after Calibration and it is recommended.	0:10:00
Basal	Not applicable	Cycles = 5 Mix = 3:00 Wait = 0:00 Measure = 3:00	0:30:00
Oligomycin / BAM15	Injection 1 (Port A)	Cycles = 10 Mix = 3:00 Wait = 0:00 Measure = 3:00	1:00:00
Rotenone + antimycin A	Injection 2 (Port B)	Cycles = 10 Mix = 3:00 Wait = 0:00 Measure = 3:00	1:00:00
	Total Time:		**3:00:00**

Table 4

Table 4.

Cell line	Seeding density (well)	Spheroid growth (days)	Final spheroid volume (μM^3)	Basal OCR (pmolO$_2$/min/well)	Sensitivity for basal OCR met (YES/NO)
SKOV	1000	5	9.52E+06	28 ± 3.5	YES
SKOV	2000	5	2.38E+07	26 ± 1.4	YES
SKOV	4000	5	4.92E+07	36 ± 3.1	YES
SKOV	8000	5	1.11E+08	50 ± 7.9	YES
HepG2	1000	5	1.11E+07	15 ± 0.7	NO
HepG2	2000	5	2.88E+07	23 ± 1.8	YES
HepG2	4000	5	5.46E+07	31 ± 1.7	YES
HepG2	8000	5	1.21E+08	52 ± 2.8	YES
A549	1000	5	2.11E+07	30 ± 2.5	YES
A549	2000	5	3.57E+07	41 ± 1.6	YES
A549	4000	5	6.93E+07	53 ± 7.2	YES
A549	8000	5	1.44E+08	65 ± 8.4	YES
MCF-7	1000	3	1.60E+07	29 ± 0.8	YES
MCF-7	2000	3	2.52E+07	37 ± 1.7	YES
MCF-7	4000	3	6.00E+07	46 ± 1.7	YES
MCF-7	8000	3	1.06E+08	66 ± 2.9	YES

Click here to access/download
Table of Materials
JoVE_Materials_list (1).xlsx

UNIVERSITY OF BIRMINGHAM

Dr. Deepika Mittal
Review Editor
JoVE

12th November, 2021

Re: Coltman et al. JoVE63346

Dear Dr Deepika Mittal,

On behalf of my co-authors, it is with great pleasure that I accept to revise our manuscript entitled "Optimised protocols to explore mitochondrial energy metabolism of single 3D microtissue spheroids using Agilent Seahorse Extracellular Flux Analysis" for publication in JoVE.

Firstly, we thank the reviewers and editors for their critical feedback on our manuscript. After consideration of the points raised by the editors and reviewers, we have taken the time to amend the manuscript accordingly as detailed in the attached rebuttal table document. We also include two manuscript files, one with tracked changes that have been made from the original manuscript document and a final manuscript document without tracked changes.

All authors agree with these revisions and approve its submission to JoVE. I look forward to hearing from you in due course, but, in the meantime, please do not hesitate to contact me if you require further information.

Yours sincerely

Dr Jonathan Barlow

Comments for editor

ID	Comments (Editor)	Author response	Change in manuscript
E-1	Please take this opportunity to thoroughly proofread the manuscript to ensure that there are no spelling or grammar issues.	The manuscript has been checked by both lead authors (Coltman and Barlow) for spelling mistakes and grammar.	No change in manuscript
E-2	Please remove the commercial term Agilent Seahorse from the title	"Agilent Seahorse" removed from title	Title amended in lines 4 -5: "Optimised protocols to explore mitochondrial energy metabolism of single 3D microtissue spheroids using Extracellular Flux Analysis"
E-3	Please revise the following lines to avoid previously published work: 144-156, 186-194, 202-209, 299-314, 347-356, 384-397	All lines will be rephrased	All lines have been rephrased or deleted where appropriate to avoid repetition from other published work – see red text in updated manuscript.
E-4	JoVE cannot publish manuscripts containing commercial language. This includes trademark symbols (™), registered symbols (®), and company names before an instrument or reagent. Please remove all commercial language from your manuscript and use generic terms instead. All commercial products should be sufficiently referenced in the Table of Materials. For example: Agilent Seahorse XFe96, XF24, Agilent Technologies, TrypLExpress, Cultrex®, Cell-Tak™, the WAVE software, GraphPad, Microsoft Excel, etc.	Commercial language will be removed from the main manuscript and referred to thereafter without such language.	Commercial products placed accordingly into table of materials

Specific commercial terms for the Agilent Seahorse XF technology are now only rereferred to once in its full-form within the Abstract (LINE 35), and in the introduction (LINE 81-82). This is to emphasise the aim of the manuscript, specific to the Agilent technology.

"Cultrex" brand name removed LINE 162

"XFe96 spheroid microplate" now referred to as: spheroid assay microplate; for cell culture this is denoted as spheroid culture plate

For some items this use of commercial language is simply unavoidable, for example where the name of the reagent item is also the brand name, e.g., TrypLExpress |
| E-5 | Please define all abbreviations upon first use. For example, 2D, RPMI, etc. | | LINE 29: two-dimensional single cell monolayers (2D culture)

RPMI defined in Materials |
| E-6 | Please provide citations (wherever appropriate) for lines 57-82. | | The manuscript has been updated to include a range of citations throughout, pertinent to not just approaches to |

			extracellular flux analyses, but also 3D cell culture in general.
E-7	Please adjust the numbering of the Protocol to follow the JoVE Instructions for Authors. For example, 1 should be followed by 1.1 and then 1.1.1 and 1.1.2 if necessary. Please refrain from using alphabets and bullets.	This has been done.	All numbering has been updated throughout to match the requested format of Jove.
E-8	Use SI units as much as possible and abbreviate all units: L, mL, µL, cm, kg, etc. Use h, min, s, for hour, minute, second.	-	MS text checked and amended where necessary. For example, all units previously written as "minutes" or "hours" have now been changed to min/h
E-9	Please ensure that all text in the protocol section is written in the imperative tense as if telling someone how to do the technique (e.g., "Do this," "Ensure that," etc.). The actions should be described in the imperative tense in complete sentences wherever possible. Avoid usage of phrases such as "could be," "should be," and "would be" throughout the Protocol. Any text that cannot be written in the imperative tense may be added as a "Note." However, notes should be concise and used sparingly. Please include all safety procedures and use of hoods, etc.		This has been checked and corrected where necessary, see red text/tracked changes.
E-10	In the JoVE Protocol format, "Notes" should be concise and used sparingly. They should only be used to provide extraneous details, optional steps, or recommendations that are not critical to a step. Any text that provides details about how to perform a particular step should either be included in the step itself or added as a sub-step.		We have taken this into consideration and made sure that any notes are more concise and essential.
E-11	The Protocol should be made up almost entirely of discrete steps without large paragraphs of text between sections.	N/A	General flow of manuscript has been updated
E-12	The Protocol should contain only action items that direct the reader to do something. Please move the discussion about the protocol to the Discussion.		This has been done
E-13	Please add more details to your protocol steps. Please ensure you answer the "how" question, i.e., how is the step performed? Alternatively, add references to published material specifying how to perform the protocol action.	LINE 123: It is assumed that standardised light/phase contrast microscopy is a 'basic' technique assumed of biological researchers reading articles in JoVe. This technique is also detailed further in "Supplemental file 1: Analysis of spheroid size and volume".	LINE 123 updated to: "Phase contrast microscopy using standardised laboratory practices". This has also been updated in section 2.1.1: "Check spheroid viability using an inverted light microscope with phase contrast at 4x magnification to ensure intact

	Line 123: Please provide details as to how the microscopic imaging was done including microscope settings, imaging parameters, magnification used, etc. Alternatively, add references to published material specifying how to perform the protocol action. Line 138: If this step needs filming, please include actions in brief how this is done.		spheroid structure, morphology, and overall uniformity between samples."
E-14	Please remove all the embedded screenshots and images from the text file. These can be uploaded as separate figures or supplemental files.	Embedded images to be removed.	Embedded images have been removed and replaced with text to describe the steps instead.
E-15	Please include a single line space between each step, substep, and note in the protocol section. Please highlight up to 3 pages of the Protocol (including headings and spacing) that identifies the essential steps of the protocol for the video, i.e., the steps that should be visualized to tell the most cohesive story of the Protocol. Remember that non-highlighted Protocol steps will remain in the manuscript, and therefore will still be available to the reader.		3 pages have been highlighted and all steps now include spaces between them.
E-16	Figure 2: Please use min to denote minutes. Please depict units as pmol/min/well, here as well as everywhere else in the manuscript and figures.	Figure formats will be updated accordingly	Units of measure changed in text from "pmol*well^{-1}*min^{-1}" to "pmol/min/well". This has also been changed in all figures and figure legends.
E-17	Figure 3: Please check the y-axis labels.		Figure 3 updated accordingly to include updates units depiction and spelling mistake corrected in panel B ("spheroid circularity"). Error bars have also been amended.
E-18	Please provide both plus and minus error bars in all the figures.		All figures have been updated in the MS including changes to y-axis. Error bars have been changed to both up- and down-direction.
E-19	As we are a methods journal, please also include in the Discussion the following in detail along with citations: a) Critical steps within the protocol b) Any limitations of the technique		The discussion has been updated to include a range of citations pertinent to not just approaches to extracellular flux analyses, but also 3D cell culture in general.
E-20	Please do not abbreviate journal names in references.	We apologise for this; it should be noted however, that we downloaded the JoVE Endnote citation format from the Journal website and installed into Endnote V.9 and thus any formatting to references was made	Journal names manually updated from abbreviated

		automatically to the citation format applied: https://www.jove.com/files/JoVE.ens	

Comments for reviewer 1

ID	Comments (Reviewer 1)	Author response	Change in manuscript
R1-1	This submission describes a detailed protocol for the real-time respirometric analysis of 3D spheroids using the Seahorse XFe96. This is a clear and detailed description of the protocol, which has not been published at this level of detail elsewhere. The authors include many useful considerations and notes for the adaptation of the protocol across different spheroid models, including notes on optimisation of cell number, poisons and normalisation. Importantly, the authors provide clear evidence of the efficacy of their protocol. Overall, this is an excellent protocol, which will find wide-interest across many different user groups.	Thank you. We have indeed tried to make the manuscript as open as possible to a broad range of users including those in academic as well as commercial environments. We have attempted to unpack as many of the steps that would be required for a 'new' user of the XF technologies , to undertake. We believe also that several of these protocols are useful to those conducting 3D cell culture experiments in general such as the importance of cell culture optimisation, and normalisation steps in these experiment types.	N/A
R1-2	In this protocol the authors employ BAM15, instead of the Agilent recommended uncoupler, FCCP/CCCP. Due to the divergence of this from the most widely used uncoupler, FCCP, the authors should provide clear reasoning, with evidence, for their choice to substitute it here.	We agree that our decision to use the protonophore, BAM15 in our XF experiments should be discussed further. We have now included more reasoning behind our choice of uncoupler. See column to the right for text that has been added to the manuscript within the discussion.	BAM15 was originally introduced as a mitochondrial uncoupler with minimal influence on plasma membranes in 2013 (59 33); with protonophoric activity in the micromolar range in whole cells and nanomolar range in isolated mitochondria. FCCP, however, depolarise mitochondrial membrane potential but also exert off target effects such as plasma membrane depolarisation. Given the potency of FCCP on plasma membrane depolarisation, BAM15 is a more reliable protonophore to uncouple respiration in intact whole cells. Although FCCP have been used for over 50 years to assay maximal respiratory capacities and continue to be used widely in XF studies, FCCP often underestimate mitochondrial and cellular metabolic capacity. This is in part linked to why so many publications using XF technology fall into the trap of reporting negative spare respiratory capacities or underestimate true mitochondrial respiratory capacities when FCCP is used. The added potency of FCCP in intact cells and tissues often leads to compromised mitochondrial function and cells can struggle to operate appropriately to sustain a maximum respiratory capacity across multiple

			measurement cycles following their addition. Therefore, the response of cells to FCCP can be found in many studies to drop off following the initial measurement cycle period. Whilst FCCP have been routinely used to conduct extracellular flux analyses, in cases where whole cells or spheroid models are concerned, BAM15 is used preferentially over these, given that it can maintain a maximum respiratory capacity in fully depolarised mitochondria at concentrations as high as 10uM. Moreover, BAM15 induces effects on extracellular acidification which coincides with that of nutrient oxidation through the hydration of CO_2 to form HCO_3- and $H+$ to a greater extent to that of FCCP. That being said, in the case of isolated mitochondria and permeabilised cells, any of these uncouplers should perform as well for mitochondrial uncoupling if titrated at the correct concentration.
R1-2	The authors rightly highlight the importance of normalisation in their protocol and provide two alternate normalisation suggestions (Supp1 and Supp2). In Supp2 they state to lyse spheroids using "spheroid lysis buffer", but there is no link to what this reagent is. Given the known difficulties in lysing spheroids, this should be information should be included.	We agree whole-heartedly with reviewer 1 that this is a key protocol and thank them for highlighting our mistake in omitting this critical information.	Protocol updated in "Supplemental file 2 - Quantification of dsDNA from spheroids in an XFe96 spheroid microplate" to include constitution of spheroid lysis buffer.
R1-3	Given the difference in potential sizes of spheroids that may be assayed by this method, have the authors considered using more than 1 spheroid per well. In the data presented, the raw OCR of some spheroids is towards the minimum OCR recommended by Agilent (20 pmol/min). In many cases, it is not possible to simply increase the number of cells per spheroid to counter this, as larger spheroids can lead to necrotic cores, or reduce the amount of time a spheroid can remain viable for thus impacting on experimental design.	Indeed, increasing the initial seeding density for spheroid cell cultures can have a significant effect on the spheroid biology output. Some researchers have found that the induction of the 'necrotic core is indeed an issue in 3D cell culture experiments and have even defined optimum cell culture parameters as such, to ensure adequate oxygen diffusion constants [1], and to maintain maximum viability. For this reason, and to assess the impact of spheroid size and cell number, we undertook as series of extracellular flux assays in a variety of spheroid types, with multiple cell number up to 8×10^3 initial cells/spheroid. Moreover it is indeed possible to add more than one spheroid into the XF spheroid microplate, we trialled this in a few	No change in manuscript.

		experiments and the system is indeed capable of delineating between rates containing 1, 2, 3 or 4 in a proportional manor. The method of adding more spheroids per/well in the spheroid microplate plate is often necessary and done with isolated pancreatic islets see publication here: https://www.ncbi.nlm.nih.gov/pubmed/30098928	
R1-4	The formatting of the tables in the pdf spanned several pages and were very difficult to view and therefore have not been reviewed.	Unfortunately, these tables were submitted in the specified format from the journal itself. Links are embedded within the journal PDF proof, for each respective table. E.g., Table 3. Mitochondrial compound concentrations… "Click here to access/download;Table;Table 3.xlsx	Journal will make tables viewable in final proof documents

Comments for reviewer 2

ID	Comments (Reviewer 2)	Author response	Change in manuscript
R2-1	The Authors provide a detailed protocol to measure mitochondrial respiration in a series of spheroids from cancer-derived cell lines with the Agilent Seahorse XFe96 Analyzer. The protocol is detailed, well-written, and will provide a useful resource for running, normalization, and analysis of spheroids in the XFe96 Extracellular Flux Analyzer using the specialized spheroid plate. Overall, I recommend publishing this review if the following remarks (all minor) are addressed by the Authors in revision:	Thank you. In this manuscript we have attempted to provide as many of the details as possible, allowing users of all levels to undertake extracellular flux analysis of 3D cell cultures using the XFe96 technology from Agilent. The optimisation steps required to achieve high-quality datasets from these assays is vast; it is hoped that this manuscript will hasten the pace at which researchers can yield the datasets required for their research questions.	N/A
R2-2	ECAR is mentioned in the introduction, but not discussed in the article about spheroid extracellular flux analysis. Do the ECAR measurements still provide information about glycolysis in spheroids in a similar manner as in 2D assays? It may be helpful to readers to add in some information about ECAR and whether the spheroid assays can be used to provide some insight into cellular metabolism, such as shifts in glycolytic and oxidative metabolism.	We agree that we have mentioned this in the introduction as we want to be transparent about what the XF technology is capable of measuring. ECAR alone is not a useful or meaningful parameter in any XF experiment since it is not corrected for the buffering capacity of the XF assay buffer nor the addition of mitochondrial acidification which arises from the hydration of CO_2 to HCO_3^- and H^+. ECAR is only insightful once these data corrections are applied and then it becomes possible to provide more accurate conclusions about glycolytic flux from them. To correct for the buffering capacity to generate more meaningful proton efflux rate (PER) data one must know the volume of the microchamber for the spheroid microplate. The manufacture has been unable to provide a true volume for this with the spheroid microplate and therefore PER data cannot be determined easily. Indeed, these measurements could be achieved empirically but this was beyond the scope of this manuscript. That said, with the right corrections and knowing the volume of the microchamber for a given spheroid size present in the well then yes ECAR data would become meaningful, and calculations of glycolytic PER could be made and XF data could then be informative for investigating both glycolytic and oxidative metabolism in spheroids.	No change in this manuscript

R2-3	The protocol states that RPMI medium should be used; can Seahorse DMEM Assay medium be used?	The Seahorse DMEM can indeed be used. During these relatively short assays (~ 3-5 hours), we found substitution with the RPMI-DMEM formulations to be of limited impact on the extracellular flux analysis. The basal formulation of the two mediums is very similar. Users can 'tune' the Seahorse RPMI mediums to match the matrix of their cell culture mediums through supplementation. Critical to the final formulation of all XF buffers and mediums, is the absence of phenol-red which is likely to interfere with the fluorescent probes within the XF probe cartridge plate. Such mediums can also be purchased from other companies and/or even be homemade. For example, Krebs ringer HEPES buffer is a simple buffer that can be used to assess respiration in many different cells including spheroid models. Just be cautions that a change in medium/buffer and its supplementation may change its overall buffering capacity and therefore if interested in ECAR the buffer factor of the medium needs to be assessed so ECAR can be transformed to PER.	No change in manuscript.
R2-3	It may be useful to include recommendations on how many replicates to include per condition to get reliable results for analysis. Exclusion criteria may also be useful especially considering the differences in respiration depending on what "well zone" the spheroid is located. Should only spheroids in Zone 1 be analyzed since basal OCR varies between zone 1 and 2?	It is true that spheroid positioning within the plate wells impacted overall values in the final datasets. As with all biological datasets, with enough replicates, such values may have limited impact on the total outcome if it is captured by the standard deviation within the assay.	We have now extended the discussion section to include statistical analyses of replicates and identifying potentially erroneous data points to be omitted. A supplementary file has been added to this effect, detailing a statistical analysis protocol "Supplementary file 3".
R2-4	Embedded images are too small and difficult to read in the protocol section.	We agree with these comments; embedded images will therefore be removed and where necessary made available as independent image files.	Embedded images have been removed and replaced with text indicating the positions for insertion in final proof for publications, e.g., "INSERT IMAGE 1" where necessary
R2-5	The tables are difficult to read as some of the columns are cut off and spread out over multiple pages.	Unfortunately, these tables were submitted in the specified format from the journal itself. Links are embedded within the journal PDF proof, for each respective table. E.g., Table 3. Mitochondrial compound concentrations... "Click here to access/download;Table;Table 3.xlsx	Journal will make tables viewable in final proof documents
R2-6	In the representative results, the volume, circularity, and basal OCR measurements are compared across groups making it very clear that these parameters can vary	This is a very good point and we have taken this comment on board. A table has been included in the manuscript to address these points.	See table 5 information.

	drastically between cell lines. This also makes it obvious that these parameters need to be optimized for every cell line. However, I think it could be useful to provide readers with some guidelines on each of these parameters and how to go about optimizing them. Rough guidelines on minimal and maximal spheroid volumes and basal OCR. How low of a basal OCR can still be analyzed? In the spheroid plate, can basal OCR get too high and risk oxygen depletion in the well?	Generally, there will always be a minimum and maximum threshold for what is recommended from the manufacture for these experiments. For the XFe96 analyser basal OCR between 20pmolso2/min/well and 200 pmolesO2/min/well are regarded as the lower and upper limits, respectively. This is the case with monolayer cells and spheroids. If you want to check the oxygen level in the well then, this data is also available from these measurements as the level data. This should be viewed routinely from each experiment for quality control purposes. If oxygen depletion in the well is occurring, then this data will show that. If this is the case then adjusting your measurement cycle may be necessary, for example increasing the mixing step so that the oxygen level in the well is recovered before the next measurement period within the measurement cycle. For single spheroid experiments using the cell lines we have explored this will be very unlikely though.	
R2-7	On line 488, the line "ATP-linked OCR in MCF-7 spheroids was lowered with oligomycin" is confusing. If I understand correctly, I think it would be better to remove ATP-linked from the sentence since oligomycin is just to determine ATP-linked respiration; therefore, OCR should be lowered with oligomycin, but that does not lower ATP-linked OCR.	Your understanding is correct, and we agree this is confusing, so we thank you for bringing this to our attention.	ATP-linked has been deleted from this line
R2-7	Figure 2/6: Why is spare capacity calculated as a percentage and not a subtraction of basal respiration from maximal respiration? While maximal respiration can be internally normalized to basal or ATP-linked respiration, spare capacity is most often presented as subtraction of basal from maximal. Is there a reason to do this differently in spheroids?	As you rightly state spare respiratory capacity is a measure of the rate of maximal mitochondrial respiratory capacity minus basal mitochondrial respiratory rate, the problem with reporting data as a rate i.e pmolO2/min/well with certain experiments is that it is not normalised to anything. Even if one normalises data to cell density/DNA content, this often excludes the key parameter that needs to be normalised for which is mitochondrial density within the cells. Given that a change in mitochondrial density will lead to a change in basal and maximal respiration proportionally, spare capacity will also increase. For example, if your basal OCR is 200 and maximum 400, spare capacity is 200, if your basal OCR is 100 and maximal 200, then your spare is 100, however as a percentage they are both 50% of maximal (or 100% of basal). Therefore, the spare	No change in manuscript

| | | capacity is not changed between these two examples, despite differences in rates of 200 and 100 when calculated as pmolsO2/min/well. To make XF data more comparable across studies and projects, internally normalised values are more reliable and insightful. To do this for spare respiratory capacity we have therefore chosen to present this as a percentage of maximal respiration instead of an absolute rate. This could also be presented as a percentage of basal respiration. This would be the case if we were working with cells or spheroids. However given that the location of the spheroid in the microwell plate may alter the absolute OCR but not the relative changes with inhibitors or uncouplers, it is more important in spheroids to look at internally normalised responses as fold change or percentages. | |

References

1   Leedale, J. *et al.* In silico-guided optimisation of oxygen gradients in hepatic spheroids. *Computational Toxicology.* **12**, doi:10.1016/j.comtox.2019.100093, (2019).

jove
JOURNAL OF VISUALIZED EXPERIMENTS

1 Alewife Center #200
Cambridge, MA 02140
tel. 617.945.9051
www.jove.com

ARTICLE LICENSE AGREEMENT

Title of Article:	Optimised protocols to explore mitochondrial energy metabolism of single 3D microtissue spheroids using Agilent Seahorse Extracellular Flux Analysis
Author(s):	Nicolas Coltman, Garret Rochford, Nikolas Hodges, Hanene Ali-Boucetta, Jonathan Barlow

Item 1: The Author elects to have the Article be made available (as described at https://www.jove.com/authors/publication) via:

[X] Standard Access   [ ] Open Access

Item 2: Please select one of the following items:

[X] The Author is **NOT** a United States government employee.

[ ] The Author is a United States government employee and the Article was prepared in the course of his or her duties as a United States government employee.

ARTICLE LICENSE AGREEMENT

1.   **Defined Terms.** As used in this Article License Agreement, the following terms shall have the following meanings: "**Agreement**" means this Article License Agreement; "**Article**" means the manuscript submitted by Author(s) and specified on the last page of this Agreement, including texts, figures, tables and abstracts; "**Author**" means the author who is a signatory to this Agreement; "**Collective Work**" means a work, such as a periodical issue, anthology or encyclopedia, in which the Article, along with a number of other contributions, constituting separate and independent works in themselves, are assembled into a collective whole;"**CRC License**" means the Creative Commons Attribution 4.0 Agreement (also known as CC-BY), the terms and conditions of which can be found at: https://creativecommons.org/licenses/by/4.0/; "**CRC NonCommercial License**" means the Creative Commons Attribution-NonCommercial 3.0 Agreement (also known as CC-BY-NC), the terms and conditions of which can be found at: http://creativecommons.org/licenses/by-nc/3.0/legalcode; "**Derivative Work**" means a work based upon the Article and other pre-existing works, such as a translation, musical arrangement, dramatization, fictionalization, motion picture version, sound recording, art reproduction, abridgment, condensation, or any other form in which the Article may be recast, transformed, or adapted; "**Institution**" means the institution, listed on the last page of this Agreement, by which the Author was employed at the time of the creation of the Article; "**JoVE**" means MyJove Corporation, a Delaware corporation and the publisher of Journal of Visualized Experiments; "**Parties**" means the Author and JoVE.

2.   **Background.** The Author, who is the author of the Article, in order to ensure the review, Internet formatting, publication, dissemination and protection of the Article, desires to have JoVE publish the Article. In furtherance of such goals, the Parties desire to memorialize in this Agreement the respective rights of each Party in and to the Article.

3.   **Grant of Rights in Article.** In consideration of JoVE agreeing to review, arrange and coordinate the peer review, format, publish and disseminate the Article, the Author hereby grants to JoVE, subject to **Sections 4** and **8** below, the exclusive, royalty-free, perpetual license (a) to publish, reproduce, distribute, display and store the Article in all forms, formats and media whether now known or hereafter developed (including without limitation in print, digital and electronic form) throughout the world, (b) to translate the Article into other languages, create adaptations, summaries or extracts of the Article or other Derivative Works or Collective Works based on all or any portion of the Article and exercise all of the rights set forth in (a) above in such translations, adaptations, summaries, extracts, Derivative Works or Collective Works and(c) to license others to do any or all of the above. The foregoing rights may be exercised in all media and formats, whether now known or hereafter devised, and include the right to make such modifications as are technically necessary to exercise the rights in other media and formats.

4.   **Retention of Rights in Article.** The Author shall, with respect to the Article, retain the non-exclusive right to use all or part of the Article for the non-commercial purpose of giving lectures, presentations or teaching classes, and to post a copy of the Article on the Institution's website or the Author's personal website, in

612542.6   For questions, please contact us at submissions@jove.com or +1.617.945.9051.

jove
JOURNAL OF
VISUALIZED EXPERIMENTS

1 Alewife Center #200
Cambridge, MA 02140
tel. 617.945.9051
www.jove.com

ARTICLE LICENSE AGREEMENT

each case provided that a link to the Article on the JoVE website is provided and notice of JoVE's copyright in the Article is included. All non-copyright intellectual property rights in and to the Article, such as patent rights, shall remain with the Author.

5. **Grant of Rights in Article – Standard Access.** This **Section 5** applies if the "Standard Access" box has been checked in **Item 1** above or if no box has been checked in **Item 1** above. In consideration of JoVE agreeing to review, arrange and coordinate the peer review, format, publish and disseminate the Article, the Author hereby acknowledges and agrees that, Subject to **Section 8** below, JoVE is and shall be the sole and exclusive owner of all rights of any nature, including, without limitation, all copyrights, in and to the Article. To the extent that, by law, the Author is deemed, now or at any time in the future, to have any rights of any nature in or to the Article, the Author hereby disclaims all such rights and transfers all such rights to JoVE.

If the Author's funding is a subject to the requirement of the NIH Public Access Policy, JoVE acknowledges that the Author retains the right to provide a copy of their final peer-reviewed manuscript to the NIH for archiving in PubMed Central 12 months after publication by JoVE. If the Author's funding is subject to the requirement of the RCUK Policy, JoVE acknowledges that the Author retains the right to self-deposit a copy of their final Accepted Manuscript in any repository, without restriction on non-commercial reuse, with a 6-month embargo, and under the CRC NonCommercial License.

Notwithstanding anything else in this agreement, if the Author's funding is a subject to the requirements of Plan S, JoVE acknowledges that the Author retains the right to provide a copy of the Author's accepted manuscript for archiving in a Plan S approved repository under a Plan S approved license.

6. **Grant of Rights in Article – Open Access.** This Section 6 applies only if the "Open Access" box has been checked in Item 1 above. If the Author's funding is subject to the requirement of the RCUK Policy, JoVE and the Author hereby grant to the public all such rights in the Article as provided in, but subject to all limitations and requirements set forth in the CRC License.

7. **Government Employees.** If the Author is a United States government employee and the Article was prepared in the course of his or her duties as a United States government employee, as indicated in **Item 2** above, and any of the licenses or grants granted by the Author hereunder exceed the scope of the 17 U.S.C. 403, then the rights granted hereunder shall be limited to the maximum rights permitted under such statute. In such case, all provisions contained herein that are not in conflict with such statute shall remain in full force and effect, and all provisions contained herein that do so conflict shall be deemed to be amended so as to provide to JoVE the maximum rights permissible within such statute.

8. **Protection of the Work.** The Author(s) authorize JoVE to take steps in the Author(s) name and on their behalf if JoVE believes some third party could be infringing or might infringe the copyright of the Article.

9. **Privacy, Personality.** The Author hereby grants JoVE the right to use the Author's name, picture, photograph, image, biography, likeness, voice and performance in any way, commercial or otherwise, in connection with the Articles and the sale, promotion and distribution thereof.

10. **Author Warranties.** The Author represents and warrants that the Article is original, that it has not been published, that the copyright interest is owned by the Author (or, if more than one author is listed at the beginning of this Agreement, by such authors collectively) and has not been assigned, licensed, or otherwise transferred to any other party. The Author represents and warrants that the author(s) listed at the top of this Agreement are the only authors of the Article. If more than one author is listed at the top of this Agreement and if any such author has not entered into a separate Article License Agreement with JoVE relating to the Article, the Author represents and warrants that the Author has been authorized by each of the other such authors to execute this Agreement on his or her behalf and to bind him or her with respect to the terms of this Agreement as if each of them had been a party hereto as an Author. The Author warrants that the use, reproduction, distribution, public or private performance or display, and/or modification of all or any portion of the Article does not and will not violate, infringe and/or misappropriate the patent, trademark, intellectual property or other rights of any third party. The Author represents and warrants that it has and will continue to comply with all government, institutional and other regulations, including, without limitation all institutional, laboratory, hospital, ethical, human and animal treatment, privacy, and all other rules, regulations, laws, procedures or guidelines, applicable to the Article, and that all research involving human and animal subjects has been approved by the Author's relevant institutional review board.

11. **JoVE Discretion.** If more than one author is listed at the beginning of this Agreement, JoVE may, in its sole discretion, elect not take any action with respect to the Article until such time as it has received complete, executed Article License Agreements from each such author. JoVE reserves the right, in its absolute and sole discretion and without giving any reason therefore, to accept or decline any work submitted to JoVE. JoVE has sole discretion as to the method of reviewing, formatting and publishing the Article, including, without limitation, to all decisions regarding timing of publication, if any.

12. **Indemnification.** The Author agrees to indemnify JoVE and/or its successors and assigns from and against any and all claims, costs, and expenses, including attorney's fees, arising out of any breach of any warranty or other representations contained herein. The Author further agrees to indemnify and hold harmless JoVE from and against any and all claims, costs, and expenses, including attorney's fees, resulting from the breach by the

jove
JOURNAL OF
VISUALIZED EXPERIMENTS

1 Alewife Center #200
Cambridge, MA 02140
tel. 617.945.9051
www.jove.com

ARTICLE LICENSE AGREEMENT

Author of any representation or warranty contained herein or from allegations or instances of violation of intellectual property rights, damage to the Author's or the Author's institution's facilities, fraud, libel, defamation, research, equipment, experiments, property damage, personal injury, violations of institutional, laboratory, hospital, ethical, human and animal treatment, privacy or other rules, regulations, laws, procedures or guidelines, liabilities and other losses or damages related in any way to the submission of work to JoVE, or publication in JoVE or elsewhere by JoVE. All indemnifications provided herein shall include JoVE's attorney's fees and costs related to said losses or damages. Such indemnification and holding harmless shall include such losses or damages incurred by, or in connection with, acts or omissions of JoVE, its employees, agents or independent contractors.

13.   **Fees.** To cover the cost incurred for its work, JoVE must receive payment before publication of the Article. Payment is due 21 days after invoice. Should the Articles not be published due to the JoVE's decision, these funds will be returned to the Author. If payment is not received before the publication of the Article, the publication will be suspended until payment is received.

14.   **Transfer, Governing Law.** This Agreement may be assigned by JoVE and shall inure to the benefits of any of JoVE's successors and assignees. This Agreement shall be governed and construed by the internal laws of the Commonwealth of Massachusetts without giving effect to any conflict of law provision thereunder. This Agreement may be executed in counterparts, each of which shall be deemed an original, but all of which together shall be deemed to me one and the same agreement. A signed copy of this Agreement delivered by facsimile, e-mail or other means of electronic transmission shall be deemed to have the same legal effect as delivery of an original signed copy of this Agreement.

A signed copy of this document must be sent with all new submissions. Only one Agreement is required per submission.

CORRESPONDING AUTHOR

Name:	Jonathan Barlow
Department:	Mitochondrial Profiling Centre
Institution:	University of Birmingham
Title:	Dr

Signature:		Date:	24.09.2021

Please submit a **signed** and **dated** copy of this license by one of the following three methods:

1. Upload an electronic version on the JoVE submission site
2. Fax the document to +1.866.381.2236
3. Mail the document to JoVE / Attn: JoVE Editorial / 1 Alewife Center #200 / Cambridge, MA 02140

Supplemental file 1: Analysis of spheroid size and volume

The following protocol assumes access to a phase-contrast microscope capable of image acquisition and a basic user knowledge of ImageJ. Proficient users can automate the following steps by creating an analysis script.

1.   Collect photomicrographs of spheroids by phase contrast microscopy, ensuring the same objective lens is used throughout. Images can also be used to confirm stability of spheroids throughout the XFe assay, e.g., spheroids dislodged during the assay may yield erroneous data (see **Figure 7**).

NOTE: Typically, a 2–4X objective lens is suitable for most 100–1,000 mM diameter spheroids.

2.   Collect photomicrographs of a known image scale.

NOTE: A simple cell culture haemocytometer is suitable as it is manufactured to known dimensions.

3.   Open ImageJ and import the hemocytometer image.

4.   Using the **Straight** annotation tool, draw a line between two known points on the hemocytometer image, e.g., each of the 16 squares within the 4 hemocytometer counting areas measures 250 μm x 250 μm (1 mm^{2}total quadrant) on the typical Neubauer-type hemocytometer.

5.   Go to **Analyse/Set scale** and set **Known distance: 250** and **Unit of length: μm.** Click to set to **Global.**

6.   Import spheroid images into ImageJ.

7.   Using the **Freehand selection** tool, draw around the circumference of each spheroid and collect data by going to **Analyse/Measure** for each spheroid.

8.   Copy **Measurement table** to clipboard and import into R', Microsoft excel, or equivalent.

9.   Use **Feret diameter** to estimate spheroid volume (mm^3) using **Feret** and **MinFeret** values according to the following equation:

Feret diameter = ((0.5) × (Feret value) × (MinFeret value^2))

NOTE: A true spheroid would have Feret/MinFeret value equal to 1; thus, these values can also be used to estimate 'roundness' of spheroids.

Supplemental file 2: Quantification of dsDNA from spheroids in an XFe96 spheroid microplate

The following steps describe a protocol for quantifying intra-spheroidal dsDNA using the Quant-iT PicoGreen dsDNA Assay Kit. As nuclear dsDNA in spheroids is linearly correlated with cell seeding density or spheroid volume (**Figure 9**), nuclear dsDNA content is a possible approach to normalize XF data. dsDNA is preferred over protein normalization, particularly where spheroid adhesion to assay culture plates is aided by poly-D-lysine and where pretreatments may impact protein synthesis.

This protocol assumes the final XFe assay well volume to be ~ 240 µL. Adjust the protocol as necessary for other volumes, e.g., spheroids within cell culture growth plates. Users may wish to prepare a standard curve of monolayer cells for DNA quantification to allow estimation of cell number within spheroids.

1.   Carefully aspirate 190 µL of XF assay medium from each well of the XFe96 spheroid microplate, leaving ~50 µL of assay medium/well.

2.   Add 50 µL/well of spheroid lysis buffer (supplemented with 20 mg/mL proteinase K), place the plate on ice, and leave to lyse for a minimum of 10–30 min.

NOTE: Shake the assay plate on a plate shaker, if necessary, to help enhance lysis. Larger spheroids may require elongated incubation, and lysis can be confirmed under the microscope. The process of freeze-thawing will also help aid spheroid lysis.

3.   Add an equal volume (100 µL/well) of 1x Tris-EDTA buffer (10 mM Tris-HCl + 1 mM EDTA, pH 7.4) to reduce sample viscosity.

4.   Carefully mix lysates within wells by pipette aspiration. Alternatively, use a plate shaker set at 500 rpm.

5.   Generate a standard curve of lambda DNA in 100 µL of XF assay medium from 2 mg/mL–2 ng/mL DNA.

6.   Add 100 µL of spheroid lysis buffer to match sample volumes and mix.

NOTE: Final standard curve will be in the range of 1 mg/mL–1 ng/mL after dilution.

7.   Transfer 20 µL of the spheroid lysate and standards into separate wells of a suitable 96-well microplate for recording fluorescence (preferably black).

8.   Dilute PicoGreen DMSO stock solution 200-fold to achieve final volume required to complete assay e.g., to achieve analysis of 10 samples at 100 µL final volume, dilute 4 µL of PicroGreen DMSO stock solution in 796 µL of 1x TE buffer.

9.   Add 80 µL/well of PicoGreen working solution and incubate at room temperature for 2–5 min, protected from light, with gentle intermittent shaking to equilibrate.

10.   Measure well fluorescence on a fluorescent-based microplate reader with an excitation wavelength of 485nm and emission wavelength of 520nm (485_{EX}–520_{EM}).

Supplemental file 3: Recommendations for the number of replicates required to obtain reliable XF assay datasets

We have shown that spheroid positioning within the XF spheroid assay microplates can impact overall values in the final datasets. As with all biological datasets, with enough replicates, such values may have limited impact on the total outcome if it is captured by the standard deviation within the assay; however, this might not always be the case. The Z' prime equation is a form of statistical analysis that compares two groups of data performing as samples or negative control. Users should therefore consider applying the Z' prime equation to subset groups of the XF data for comparison. Unlike other statistical test such as standardized mean difference (SSMD)[1], the Z' primes formula is not robust to outliers[2] and is therefore ideally placed to help users identify erroneous XF assay datapoints or datapoints that do not fit the dispersion of other replicates within the group, as might be the case with the misalignment of spheroids in the assay microplate .

$$Z' = 1 - \frac{3\sigma_{positive\ control\ values} + 3\sigma_{negative\ control\ values}}{|\mu_{positive\ control\ values} - \mu_{negative\ control\ values}|}$$

$3\sigma_{positive\ control\ values} = 3 \times$ standard deviation of sample values in XF assays
$3\sigma_{negative\ control\ values} = 3 \times$ standard deviation of control wells values in XF assays
$\mu_{positive\ control\ values} =$ mean of sample values in XF assays
$\mu_{negative\ control\ values} =$ mean of control wells values in XF assays

Supplemental Figure S1: Derivation of the Z' primes equation.

The above equation states that good Z' values can only be obtained when all values, representing both upper and lower, are sufficiently different from each other. In this way, applied to XF data, the 'signal' intensity of both value sets should be significant enough to separate them and the standard deviation should be as low as possible. For example, a strong Z' prime value could be achieved with a large signal discrimination or with tight dispersion of values attributed to the standard deviation.

1.   Collect values for sample replicate wells (representing positive control values) and for the background correction wells (representing negative control values).

2.   Derive the mean average and standard deviation for both data groups.

3.   Apply the Z' primes equation.

Supplemental Table S1: Interpretation of Z' prime values.

Z' primes value (z-factor)	Data interpretation
1.0	Ideal value but should not exceed
$\geq 0.5 - \leq 1.0$	Good discrimination between data groups
$\geq 0 - \leq 0.5$	Questionable separation between groups
> 0	The overlap between the control and sample wells is too great.

4.   To determine the impact of a particular well on the overall dataset, users should omit those values of interest and see how Z' primes is altered. For example, outliers in either data group will affect the Z' primes output.

Using power analysis, Yépez et al. highlight the ideal number of replicates in the XFe96 format to be 12 per sample type[3]. Within the context of 3D cell culture, which is often limited by the amount of material available (e.g., cost of 3D cell culture; maintenance of samples), we believe this to be unrealistic and recommend 5–8 samples per condition measured.

References

1   Zhang, X. D. et al. The use of strictly standardized mean difference for hit selection in primary RNA interference high-throughput screening experiments. *Journal of Biomolecular Screening.* **12** (4), 497–509 (2007).
2   Zhang, J. H., Chung, T. D., Oldenburg, K. R. A simple statistical parameter for use in evaluation and validation of high throughput screening assays. *Journal of Biomoecularl Screening.* **4** (2), 67–73 (1999).
3   Yepez, V. A. et al. OCR-Stats: Robust estimation and statistical testing of mitochondrial respiration activities using Seahorse XF Analyzer. *PLoS One.* **13** (7), e0199938 (2018).